Long-range directional growth of neurites induced by magnetic forces

Tasmin Nahar, Monte Gates, Emilie Secret, Jean-Michel Siaugue, Jérôme Fresnais, Michael Rotherham, Heidi R Fuller, Sharon J Brown, Alicia J El Haj, Neil D Telling

Acta Biomaterialia xxx (xxxx) xxx

Contents lists available at ScienceDirect

Acta Biomaterialia

journal homepage: www.elsevier.com/locate/actbio

Full length article

Long-range directional growth of neurites induced by magnetic forces

Tasmin Nahar [a], Monte Gates [a,b], Emilie Secret [c], Jean-Michel Siaugue [c], Jérôme Fresnais [c], Michael Rotherham [a,d], Heidi R. Fuller [e], Sharon J. Brown [a], Alicia J. El Haj [d], Neil D. Telling [a,*]

[a] School of Life Sciences, Keele University, Staffordshire, UK
[b] School of Medicine, Keele University, Staffordshire, UK
[c] Sorbonne Université, CNRS, Physico-Chimie des Électrolytes et Nanosystèmes Interfaciaux, PHENIX, 75005, Paris, France
[d] Healthcare Technologies Institute, Institute of Translational Medicine, School of Chemical Engineering, University of Birmingham, Birmingham, United Kingdom
[e] School of Allied Health Professions and Pharmacy, Keele University, Staffordshire, UK

ARTICLE INFO

Keywords:
Neurite growth
Magnetic nanoparticles
Magnetic forces
Magnetogenetics
Neuroregeneration

ABSTRACT

The ability to control the growth and orientation of neurites over long distances has significant implications for regenerative therapies and the development of physiologically relevant brain tissue models. In this study, the forces generated on magnetic nanoparticles internalised within intracellular endosomes are used to direct the orientation of neuronal outgrowth in cell cultures. Following differentiation, neurite orientation was observed after 3 days application of magnetic forces to human neuroblastoma (SH-SY5Y) cells, and after 4 days application to rat cortical primary neurons. The direction of neurite outgrowth was quantified using a 2D Fourier transform analysis, showing agreement with the derived magnetic force vectors. Orientation control was found to be effective over areas >1cm^2 using modest forces of ~10 fN per endosome, apparently limited only by the local confluence of the cells. A bioinformatics analysis of protein expression in cells exposed to magnetic forces revealed changes to cell signaling and metabolic pathways resulting in enhanced carbohydrate metabolism, as well as the perturbation of processes related to cellular organisation and proliferation. Additionally, in cell culture regions where the measured force vectors converged, large (~100 μm) SH-SY5Y neuroclusters loaded with nanoparticles were found, connected by unusually thick linear neurite fibres. This could suggest a magnetically driven enhancement of neurocluster growth, with the clusters themselves contributing to the local forces that direct outgrowth. Such structures, which have not been previously observed, could provide new insights into the development and possible enhancement of neural circuitry.

Statement of Significance: A magnetic force approach for directing outgrowth in neuronal cells over macroscopic areas is successfully demonstrated. Cells were incubated with magnetic nanoparticles which were sequestered into intracellular compartments. Permanent magnet arrays created local intracellular magnetic force vectors mediated via the internalized nanoparticles, which were found to precisely guide neurite orientation. Analysis of cellular protein expression suggested the mechanism for directed growth involved specific cell signaling and metabolic pathways. In addition, highly unusual straight and thick neural fibers were observed that connected large 'magnetic' spherical cell clusters. The results reported will advance nanotechnology and cell therapy for neuro-regeneration where magnetic forces could help to reconnect damaged neurons, or even build artificial neuronal architectures.

1. Introduction

Neurodegenerative diseases such as Parkinson's disease affect millions worldwide, with pharmaceutical interventions so far failing to provide cures [1]. Regenerative medicine approaches have been actively considered as alternative treatments in this area for some time. Nanotechnology based regenerative medicine methods include the manipulation of cellular processes towards a desired direction, or remote control of intrinsic and extrinsic cell structures using small nanoscale structures [2–4]. However, these approaches require the transplantation

* Corresponding author.
E-mail address: n.d.telling@keele.ac.uk (N.D. Telling).

https://doi.org/10.1016/j.actbio.2024.12.057
Received 23 July 2023; Received in revised form 23 December 2024; Accepted 26 December 2024
Available online 2 January 2025

of dopaminergic neurons into the area of disease, and previous studies have been unable to show the re-establishment of the neuronal circuits [5,6] required to restore brain function.

A crucial step towards re-establishing neuronal circuitry is the ability to manipulate axon growth. The mechanical stimuli that drive outgrowth and elongation of developing axons are not fully understood. However, the balance between forces generated within the growth cone and axonal shaft is known to play a key role [7,8]. Of the different extrinsic forces that could modulate these processes, the application of weak forces (<1 nN) over longer time periods (days to weeks) has been found to promote axonal outgrowth [7], with such forces resembling the weak endogenous forces that are essential for nervous system development [9].

The enhancement of axon growth using mechanical forces is a process commonly referred to as 'stretch-growth' [10,11]. The potential to both study and manipulate axon growth using mechanical stimuli has been an active area of research for many years, with the methods used ranging from direct mechanical manipulation of the growth cone using microneedles [12,13] and optical or magnetic tweezers [14,15], to methods that manipulate adherent cells via substrate movement [16, 17].

The mechanical manipulation of neuronal cell processes can also be achieved remotely and without direct contact, through the use of magnetic nanoparticles (MNPs).These have proven to be a useful tool in the field of biomedicine due to their biocompatibility and cell modulating properties [18–20]. Sometimes referred to as magnetogenetics, such methods have arisen as an approach to remotely control specific signalling pathways, for example by functionalising MNPs to a target mechano-receptor [21–23]. Although a promising tool, the brain is a complex system with a variety of signalling cascades and further research is required to determine target receptor complexes which can control neuronal circuitry [24].

Despite these challenges, MNP mediated mechanical and physical stimuli have been shown to exert cytoskeletal changes, as well as affecting cell migration and polarity [25–28]. Non-specific spatiotemporal MNP routes have also been explored, although these relied on topographical cues on the cell substrate [29] or microfluidic devices to study control of neurite outgrowth [30]. Therefore, it is unclear whether the growth observed was due to the influence of a magnetic field through the action of MNPs, or simply the biochemical and physical influence of the platforms used to study these effects [29–32].

A recent study also demonstrated that magneto-mechanical forces can stimulate axon growth using a process described by the authors as "magnetic nano-pulling" [33]. This study focused on unravelling the axonal growth mechanisms that lead to axon elongation through intercalated mass addition under stretching with very weak (~pN) magnetic forces. The authors proposed a model whereby nano-pulling promoted the stabilization of microtubules in growing axons, ultimately activating local translation to supply the necessary proteins and associated vesicles required to sustain axon outgrowth. Principal component analysis following RNA sequencing of axons, revealed the involvement of genes related to cytoskeleton and synapse remodelling, suggesting that the stretching also enhanced neuronal maturation. This study also indicated that mechanical stimulation actuated by weak magnetic forces, may speed up synapse formation and development towards maturation. This is important for potential applications using magnetic stretching to reconstitute neural circuitry, as regaining functionality also requires the restoration of synaptic signalling.

Complementary to this, novel tools such as optogenetics have made great advances for understanding and manipulating neuronal activity, as well as offering potential methods to bypass synaptic defects [17]. For neuro-regenerative studies optogenetics does have some drawbacks: for instance, light may not penetrate to the required depth within the tissue and in addition could produce local heating effects and non-specific toxicity [34]. To mitigate this, recent approaches for stimulating deep brain areas have explored the direct targeting of light sensitive cells using internal light generation methods, such as bioluminescence [35].

In a previous study we demonstrated that neuronal outgrowth could be directed towards magnetic microstructures as a result of the packing of intracellular endosomes with MNPs, thereby driving cellular actuation [24]. However, this work focused on individual cells observed over short time scales, rather than assessing the longer-term growth of cell populations. Similarly, other studies have successfully demonstrated induced directionality in neuronal outgrowth over short distances local to the cell bodies [24,31,32,36–39].

Here, we report a spatially controlled magnetic force approach to direct neuronal outgrowth following endosomal packing with MNPs, demonstrating results in both an immortalised neuronal cell line (SH-SY5Y), and in primary rat cortical neurons. It is possible that magnetic force vectors could induce anisotropy in the overall mechanical cues experienced by cells in the vicinity of these forces, thus influencing the local direction of neurite outgrowth. To observe such effects, rather than focusing on the response of individual cells, or directly assessing the elongation of axons under magnetic stretching, we instead explore how local variations in the direction and magnitude of the forces affect the orientational growth of neurites in cell populations.

To test the correlation between local magnetic force direction and orientation of neurites, we used a simple permanent magnet array that was positioned under cell culture plates. The arrangement of the magnets in the array was chosen to produce a pattern in the orientation of magnetic forces that could be reflected in the subsequent neurite growth. By mapping the neurite outgrowth in cell populations covering regions where both the direction and magnitude of the magnetic forces varied, we show how even very weak magnetic forces are sufficient to uniformly align neurites in large populations of neuronal cells over areas of ~1 cm^2. We also show the unexpected formation of large clusters of neuronal cells in specific regions, which are connected by unusually thick and linear neurite fibres.

2. Experimental section

2.1. Cell culture

In all instances, cells were seeded on tissue culture vessels pre - coated in laminin diluted 5μg/ml in phosphate buffer saline (PBS) (Scientific laboratory supplies limited) and poly-L-ornithine (Sigma) diluted 20μg/ml in sterile dH_20 and incubated at 37°C and 5 % CO_2.

The human SH-SY5Y cell line were maintained in DMEM F-12 (Corning), supplemented with 10 % FBS, 1 % antibiotic-antimycotic (Gibco). Cells were differentiated towards a neuronal like phenotype using 10 μm retinoic acid (RA) and 50 ng/ml brain derived neurotrophic growth factor (BDNF). On day 7 of differentiation, cells underwent supplementation with MNPs corresponding in an iron concentration of 3 mM pre incubated in serum free media containing BDNF and RA. Cell labelling was performed over 24 hrs at 37 °C, with subsequent PBS washes to remove unbound particles.

Cell culture plates were then positioned directly on top of a magnet array which comprised of stacks of 6 mm diameter NdFeB permanent magnets, positioned in a regular array of holes in an aluminium plate (see Scheme 1). The cell culture plate position was such that the cell monolayer was 1 mm above the surface of the disc magnets. The cells were cultured in this arrangement for 3 days or 3 weeks.

For primary cell studies; long-distant, cortical projection neurons were dissected from a region of the E17 rat brain (day of plugging = E0) approximating the immature primary motor cortex. Meninges from the tissue were carefully peeled away in cold Neurobasal buffer, with the aid of a dissection microscope. Cells were triturated approximately 20 times using a standard 200 μl pipette tip to obtain single cells suspension. The primary rat cortical neurons were grown on coated 6 well plates and cultured in Neurobasal-based medium (Thermofisher), containing 10 % FBS, 1 % Glutamax (Thermofisher), 1 % B27 (Thermofisher), 1x pen/strp/fungizone (Thermofisher) and 1.5 % glucose (Sigma). MNPs

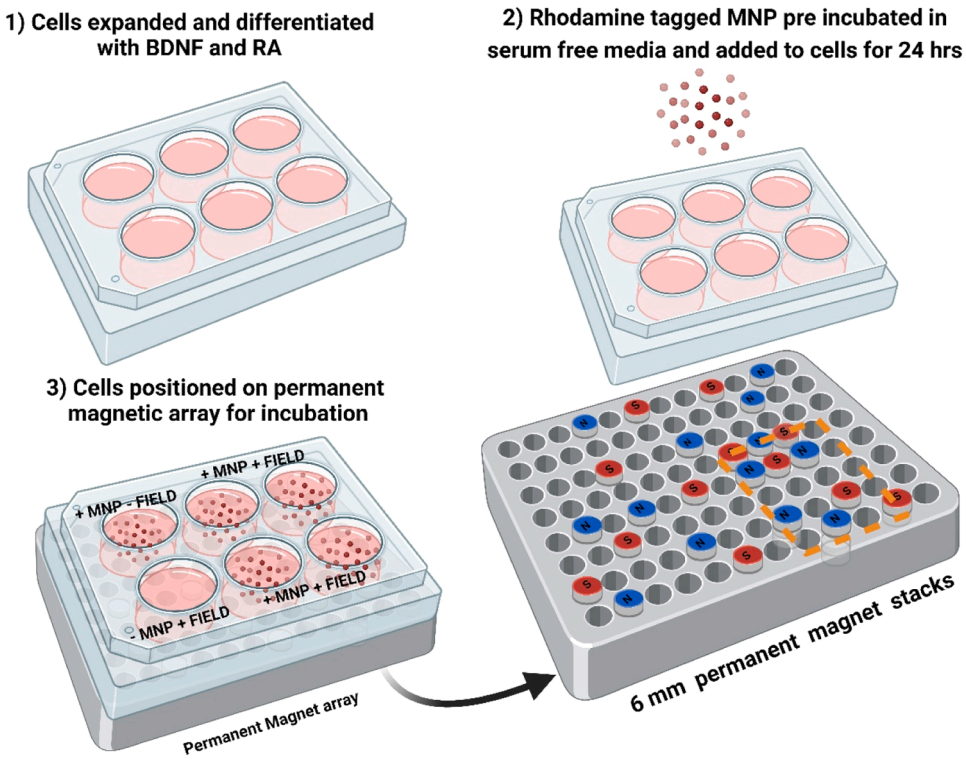

Scheme 1. Summary of experimental methodology for culture of neuronal cells loaded with fluorescently tagged magnetic nanoparticles (MNPs) exposed to variable magnetic fields. The orange dashed area shown on the permanent magnet array image indicates the region where magnetic forces were compared to images of cell and neurite growth. BDNF - Brain Derived Neurotrophic Factor; RA – Retinoic Acid.

corresponding to an iron concentration of 1 mM were pre incubated in Neurobasal medium, supplemented with 1 % B27, 1 % antibiotic-antimycotic and 1 % Glutamax were added to the cells after 48 hrs. Cells were then positioned directly above the magnetic array for 4 days and fixed with 4 % PFA.

2.2. MNP synthesis and characterisation

The sorted maghemite nanoparticles were synthesized by an inverse co-precipitation method. The acidic iron (II) and iron (III) ions solution (250 g of $FeCl_2$,$4H_2O$, 50 mL of HCl 37 %, 250 mL of deionized (DI) water, 176 mL of $FeCl_3$ 27 %) was added dropwise over 30 h into 2 L of 5 % ammonia in water under agitation. This procedure is in favour of a short nucleation process and a more pronounced growth of the particles to reach larger particle sizes. After rinsing the obtained Fe_3O_4 nanoparticles, they were oxidized into γ-Fe_2O_3 nanoparticles by boiling them with a solution of iron (III) nitrate (200 g of $Fe(NO_3)_3$ in 500 mL of DI water) for 30 min. After several washing steps, the nanoparticles were finally size sorted by gradually adding nitric acid to increase the ionic strength of the solution and thus make the larger particles flocculate to decrease their polydispersity. At this stage, a dispersion of maghemite an iron concentration of 0.52 M was obtained.

The particles were then functionalized with rhodamine B to make them fluorescent and with poly(acrylic acid) to keep them colloidally stable in biological media. To functionalize the maghemite nanoparticles with rhodamine B, first 0.3 g of amino-PEG-phosphonic acid hydrochloride (phosph-PEG-NH_2, Mw = 2100 g/mol, Specific polymers, Castries, France) were dissolved in 59.7 g of DI water. The pH of the solution was brought to 8.5 with 30 % ammonia. Then, 1.53 mL of a 10 mg/mL solution of rhodamine B isothiocyanate was added to the phosph-PEG-NH_2 solution. The solution was agitated for two days, and the pH of this phosph-PEG-Rho solution was finally brought to 2 by the addition of nitric acid. 52.2 g of this solution was slowly added to 148 g of the dispersion of maghemite nanoparticles previously diluted to be at 1 wt% (percentage by weight). After 10 min of agitation, the nanoparticles were then added dropwise to 266 g of a solution of poly(acrylic acid) (PAA8k, Mw = 8000 g/mol) at 1 wt% at pH=2. The MNPs were then magnetically removed from the solution and redispersed in a 20 % ammonia solution. They were then dialyzed against DI water 5 times and finally redispersed in a 200 mM HEPES buffer at pH=7.4.

The obtained maghemite nanoparticles were characterized by transmission electron microscopy (TEM) on a JEOL 1011 instrument, by dynamic light scattering (DLS) on a Malvern Zetasizer Nano ZS and by superconducting quantum interference device (SQUID) magnetometry on a Quantum Design MPMS-XL instrument at the platform “Mesures Physiques à Basses Températures” of Sorbonne Université. The results of this characterization can be seen in Figure S3. The average physical diameter, measured by measuring over 700 particles on ImageJ is 17.4 nm. The mean hydrodynamic sizes of the particles dispersed in the HEPES buffer is 73.6 nm, with a polydispersity index of 0.209. Finally, the MNPs are superparamagnetic with a saturation magnetization of 60 emu/g.

2.3. Immunofluorescence

Samples were fixed with 4 % paraformaldehyde (PFA, Sigma), and permeabilised with Triton-X100 (Sigma) diluted 1:1000 in PBS for 10 min. Cells were then blocked with 2 % BSA (Fisher) in PBS for 2 h Cells were then stained with anti βIII – Tubulin antibody (Abcam) diluted 1:1000 in 1 % BSA in PBS overnight. Followed by PBS washes and staining for secondary antibody anti-mouse FITC (Sigma) diluted 1:1000 in 1 % BSA in PBS for 1 hour. Cells were then counterstained with DAPI for 15 min and imaged.

2.4. XTT assay

Cells were seeded onto 96 well plate at a density of 10^3 cells per well for MNP loading at day 3 and day 21 respectively. The cells were then

expanded and differentiated as described previously. On day 7 of differentiation, cells were supplemented with medium containing particles ranging from 0.078 mM – 10 mM. Samples were tested in quadruplicates. Upon day 3 and day 21 of MNP incubation an XTT assay was conducted (ab232856, Abcam) according to the manufacturer's guidance and absorbance was read at 450 nm.

2.5. Characterisation of magnetic field gradients

To determine the magnetic force vectors on the nanoparticles in the cells, the magnetic field generated across the permanent magnet array was measured using a 3D magnetic field mapping system that utilises a 3-axis Hall probe (Senis AG, M3D-2A-PORT). As described earlier, the cell monolayer was positioned 1 mm above the surfaces of the permanent magnets during the cell culture experiments. Magnetic field gradients in this XY plane (*i.e.*, the plane containing the cell monolayer) were determined by measuring the X and Y components of the magnetic field intensity, H, across regions of interest at a height of 1 mm above the permanent magnets. From these magnetic field intensity measurements, a Matlab script was used to calculate the X and Y components of the magnetic field gradient as a function of position within this plane.

The vertical (Z) component of the field gradient was determined by repeating the magnetic field measurements at a height 0.5 mm above the original position, and dividing the difference in the Z component of the field at the two positions by the vertical displacement (*i.e.*, 0.5 mm). Ideally, measurements would have been performed at equal vertical displacements above and below the plane at which the cells were positioned. However, due to geometrical constraints, it was not possible to move the Hall effect sensor closer than 0.9 mm to the magnet surfaces, and so the Z component of the field gradient determined here is slightly inaccurate as it represents the values in the plane 0.25 mm above the position of the cell layer. The X, Y and Z components of the field gradient determined above were combined to give the overall (X,Y) position-dependent magnetic field intensity gradient, ∇H, within the cell plane ($Z = 1$ mm).

2.6. Image acquisition and analysis

Fluorescence microscopy was performed using a Nikon eclipse Ti-S operating Micro – manager 1.4 software. Representative images of $n = 3$ are shown. The larger stitch area ($n = 1$) was imaged using a detachable cell counting grid (STEMgrid™-6; Stem cell technologies) for six well dishes. Each grid represents a 2×2 mm square, which covers the entire well. Images were analysed using the Image J software to obtain 2D Fourier transforms (2D-FT) of fluorescence or bright field images. The Oval Profile plugin (authored by Bill O'Connell, http://rsb. info.nih. gov/ij/plugins/oval-profile.html) was used to obtain radial sum plots from the 2D-FTs, taking 300 data points around the complete circle. The final radial sum plots presented were filtered using an 11-point sliding window smoothing to improve visibility of the broad peaks associated with average neurite alignment.

Sample preparation for sequential window acquisition of all theoretical fragment ion spectra (SWATH)- mass spectrometry determination: Samples were collected for proteomic analysis by washing with PBS and addition of trypsin. Upon detachment, 500 µl of DMEM containing 10 % FBS was added to the wells and the cells harvested into 1.5 ml eppendorf tubes. The cells were then spun down at 365 x *g* for 6 mins. Upon centrifugation, the supernatant was discarded, and the pellet immediately frozen at −80 °C.

Cell pellets were extracted by resuspending in 3–4 vol (w/v) in 8 M urea dissolved in 100 mM ammonium bicarbonate in sterile distilled water plus 2 % sodium deoxycholate, left on ice for ~5 −10 min, and sonicated using a Soniprep 150 for 10 s at a setting of 5 amplitude microns. Samples were centrifuged at 13,000 RPM (MSE, Heathfield, UK; MSB010.CX2.5 Micro Centaur) at 4 °C for 5 min to pellet insoluble material. Using a Pierce™ BCA Protein Assay Kit (23,227; ThermoScientific), the protein concentrations of the cell extractions were calculated. A FLUOstar Omega microplate reader (BMG LABTECH) was used to read the absorbance at 562 nm and a standard calibration curve derived from a plot of the average-blank corrected absorbance *versus* concentration for each of the standards.

A 50 µg aliquot of each sample was diluted with 8 M urea/2 % sodium deoxycholate in 100 mM ammonium bicarbonate to obtain equal concentration and reduced with Tris (2-carboxyethyl) phosphine (5 mM) at 30 °C for 1 h followed by alkylation with iodoacetamide (10 mM) in the dark at room temperature for 30 min. Following reaction quenching with 20 mM DTT, each sample was digested with trypsin (1:50; protease:protein) overnight. Peptides were taken to clean-up by C-18, then dried and resuspended to 1 µg/µl in loading buffer (100 % water, 0.1 % formic acid). Data independent acquisition was performed on individual samples (DIA-MS). In addition, a pool of all the samples was prepared, and a portion subjected to nanoLC MS/MS analysis using data dependent acquisition (DDA-MS). The remaining pooled sample was then fractionated on high-pH C-18 reverse-phase into 12 fractions before analysing the fractions individually in DDA mode.

DIA data was quantified using Skyline ((64bit) version 21.2.0.369) with a customised library created from all DDA spectra. DIA data was then imported and reintegrated and quantified based on the peak scoring model of MSProphet.

2.7. Data dependent acquisition (DDA)

Peptides (5 µg) were subjected to LCMS/MS using an Ultimate 3000 RSLC (Thermo Fisher Scientific) coupled to an Orbitrap Fusion Lumos Tribrid mass spectrometer (Thermo Fisher Scientific). Peptides were injected onto a reverse-phase trap (Pepmap100 C18 5 µm 0.3 × 5 mm) for pre-concentration and desalted with loading buffer, at 5 µL/min for 10 min. The peptide trap was then switched into line with the analytical column (Easy-spray Pepmap RSLC C18 2 µm, 50 cm x75 µm ID). Peptides were eluted from the column using a linear solvent gradient: linear 4–40 % of buffer B (mobile phase A: 99.9 % water and 0.1 % formic acid; mobile phase B: 80 % acetonitrile, 20 % water and 0.1 % formic acid) over 120 min, linear 40–60 % of buffer B for 30 min, sharp increase to 95 % buffer B within 0.1 min, isocratic 95 % of buffer B for 15 min, sharp decrease to 2 % buffer B within 0.1 min and isocratic 2 % buffer B for 15 min. The mass spectrometer was operated in DDA positive ion mode with a cycle time of 1.5 s. The Orbitrap was selected as the MS1 detector at a resolution of 120,000 with a scan range of m/z 375 to 1500. Peptides with charge states 2 to 5 were selected for fragmentation in the ion trap using HCD as collision energy.

The raw data files were converted into mgf using MSconvert (ProteoWizard) and searched using Mascot with trypsin as the cleavage enzyme and carbamidomethylation as a fixed modification of cysteines against the Swissprot database, restricted only to proteins from humans. Note that the iRT peptides were added to this database. The mass accuracy for the MS scan was set to 20 ppm and for the fragment ion mass to 0.6 Da Trypsin was selected as the enzyme with 1 missed cleavage allowed. Carbamidomethylation was set as fixed and oxidised methionine as a variable modification.

2.8. Data independent acquisition (DIA mode)

Sample (5 µg) was injected onto the same LCMS set up as above with the same gradient, however data acquisition was done in DIA mode. The DIA MS method alternates between a MS scan and a tMS2 scan containing 24 scan windows. The MS scan has the following parameters: the Orbitrap at 120,000 resolution is selected as detector with a m/z range from 400 to 1000. The tMS2 scan uses HCD as activation energy with fragments detected in the Orbitrap at 30,000 resolution. The first 20 m/z windows are 20 mass units wide from 410 to 790 followed by a 30 m/z window from 790 to 820, a 40 m/z window from 820 to 860, a 50 m/z window from 860 to 910 and a 60 m/z window from 910 to 970. DIA

data was quantified using Skyline ((64-bit) version 21.2.0.369) with a customised library created from all DDA spectra. DIA data was then imported and reintegrated and quantified based on the peak scoring model of MSProphet.

Bioinformatics analysis of differentially expressed proteins: Following mass spectrometry analysis, the data was filtered to include proteins identified from ≥2 peptides that were significantly ($p \leq 0.01$) changed in expression by either 25 % or 50 % between SH-SY5Y cells loaded with MNPs and exposed to magnetic fields, and control cells. Next, Ingenuity Pathway Analysis (IPA) software was used to identify enriched cellular processes and pathways with which the differentially expressed proteins are associated. A p-value was determined using the right-tailed Fisher's Exact Test to assess the likelihood that the association of each cellular or molecular function with its corresponding set of proteins is a result of random chance.

2.9. Statistical analysis

To process data from the XTT assay, statistical analysis was performed to compare cell metabolic activity on cells N = 4, (measured via absorbance at 450 nm) at Day 3 and Day 21 for various MNP concentrations. A paired *t*-test was chosen for this analysis because the same samples were measured at two different time points (Day 3 and Day 21) for each concentration of MNPs. Normality was assessed using the Shapiro-Wilk test, which confirmed that the data for each concentration was approximately normally distributed ($p < 0.05$).

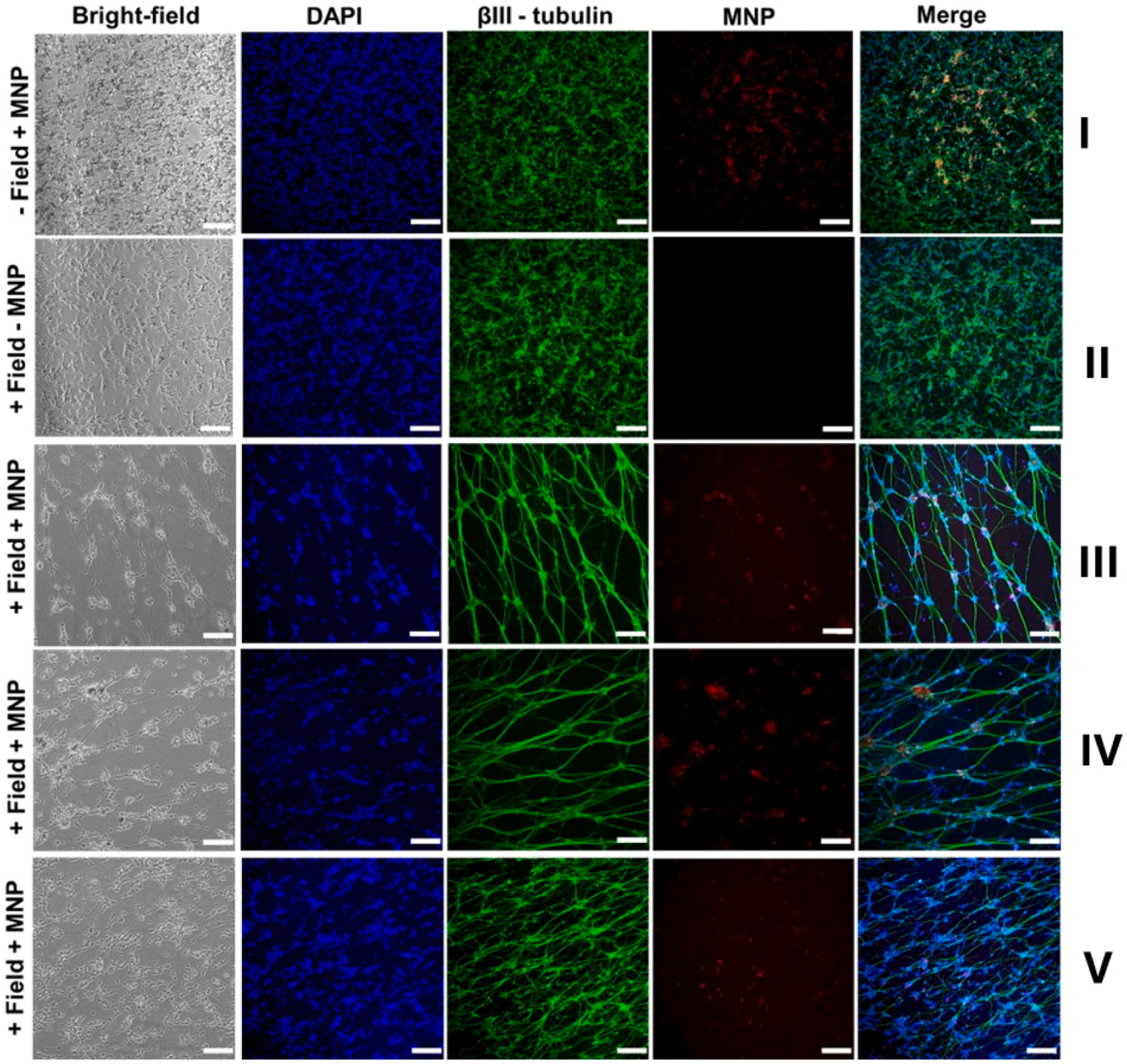

Fig. 1. Bright field (first column) and fluorescence microscopy images of SH-SY5Y cells cultured under different magnetic field exposure conditions and subsequently fixed at 2 weeks after MNP loading. Nuclear staining to show cell locations was performed using DAPI (4′,6-diamidino-2-phenylindole) (blue), with neurons (and associated outgrowths) stained using a β-III tubulin fluorescent antibody (green), whilst magnetic nanoparticles (MNPs) could be observed due to their conjugation to a rhodamine fluorescent dye (red). Controls are shown in rows I and II, whilst rows III, IV and V are cells grown in different positions on the magnet array. A further control obtained from unloaded cells in the absence of the magnetic field (- Field – MNP) is shown in Fig. 3a. Scale bars = 200 μm.

To analyze the changes in protein expression between the experimental and control groups for the proteomic experiments, multiple unpaired t-tests with Welch correction were carried out assuming individual variance for each group and applying no correction for multiple comparisons.

3. Results and discussion

To explore the effect of magnetic forces on neurite outgrowth, a simple *in vitro* experimental method was employed in which expanded and differentiated neuronal-like cells (the human derived cell line, SH-SY5Y) were loaded with fluorescently tagged MNPs, and subsequently cultured directly on top of an aluminium plate with an array of holes containing permanent magnets (Scheme 1). The permanent magnets were arranged as stacks of 6 mm discs, which could be positioned in different holes in the plate to obtain different magnetic field configurations. The permanent magnets could also be completely removed from areas of the array plate for zero field controls ('- Field + MNP'), with additional controls provided in the form of unloaded cells ('+ Field - MNP' and '-Field - MNP').

In an initial experiment, MNP loaded cells exposed to magnetic fields for 2 weeks after nanoparticle labelling, were compared to controls (Fig. 1). Both cells loaded with MNPs but without exposure to a magnetic field (Fig. 1, row I) and unloaded cells exposed to the magnetic field (Fig. 1, row II), show typical morphology for these cells with a random orientation of neurite outgrowth. However, for MNP loaded cells that were exposed to a magnetic field, a clear directional orientation of neuronal outgrowth is visible (Fig. 1, rows III-V)). The reproducibility of this orientational effect was confirmed even for cells cultured many months apart (Figure S1). It is evident that there is aggregation of cells to form neuroclusters in all samples, and less confluent areas appear to develop thicker but more sparse neurite outgrowth (Fig. 1, rows III,IV) whilst more confluent regions (Fig. 1, row V) show similar orientation but have thinner and more densely packed neurite outgrowth (see also for example, Figure S1, position 3).

In our previous study using the same cell type and similar MNPs, we found that endosomal accumulation of nanoparticles produced large intracellular magnetic clusters, containing up to several thousand superparamagnetic particles [24]. For this earlier study, strong magnetic field gradients were generated using a 100μm magnetic pillar array positioned within a uniform magnetic field. The forces on the endosomal magnetic clusters in cells grown directly onto this array, induced by these strong magnetic field gradients, were determined to be in the range of ~100 s fN per endosome. These forces were found to be sufficient to drag developing neurites as well as non-adherent cells towards the pillars in the magnetic array. However, owing to the size of the pillars, forces of this magnitude extended to only a few 10 s of micrometres from the surface of the pillars.

To confirm the same uptake mechanism for the MNPs and the cells used here, we performed TEM analysis on cells following incubation with nanoparticles. Some example images are shown in Figure S2 and clearly reveal that endosomal accumulation occurred. From measurements of the endosomal sizes seen in these images, it was also possible to estimate the approximate number of MNPs contained within each endosome (table S1), which dictates the magnetic forces on the MNP filled endosomes. Building on observations from the previous study mentioned above, it appears likely that the aligned neurite outgrowth witnessed here is the result of forces acting on these magnetic endosomes. Higher magnification images of MNP loaded cells grown during magnetic field exposure (Fig. 2) indicate some fluorescence in the MNP channel (rhodamine) along the lengths of the neurites. This could indicate the presence of some residual MNPs within the neurites themselves following outgrowth as has been observed previously [23], although here it is difficult to rule out artefacts such as autofluorescence and scattering caused by the neurite structure. In addition, it can be seen from the figure that the neuroclusters formed are comprised of cells that show a high loading of MNPs.

It was our original intention to look for patterns in the behaviour of neurite growth that reflected the arrangement of the magnets and consequent local variations in the force orientation. However, variability in cell seeding density and subsequent growth, resulted in dense populations of cells confined to specific regions within cell culture wells.

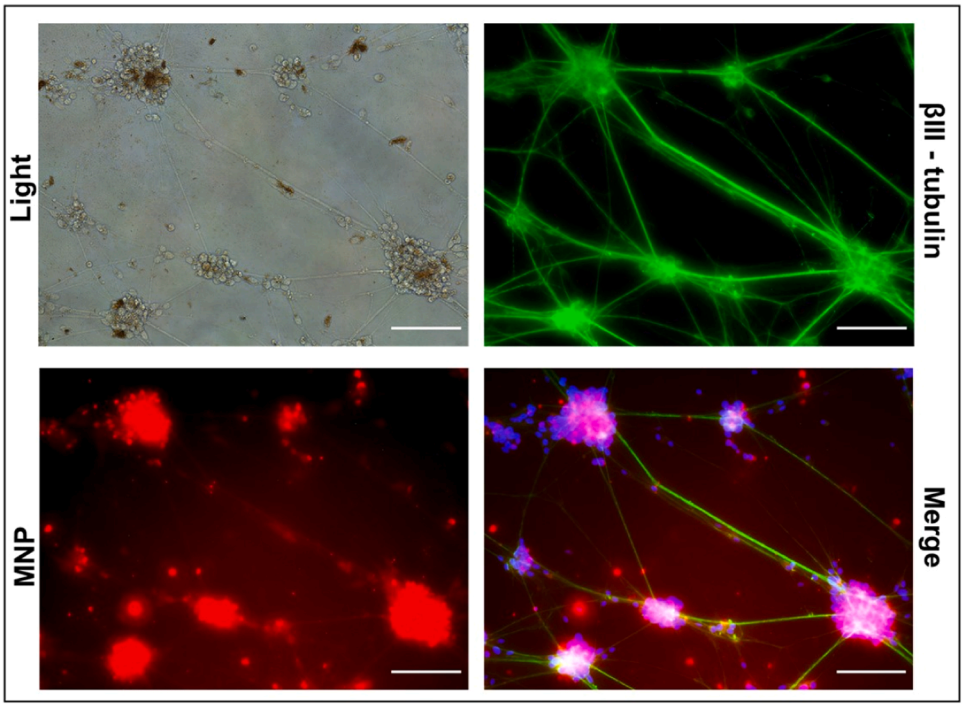

Fig. 2. High magnification bright field and fluorescence microscopy images of SH-SY5Y cells cultured under magnetic field exposure. Nuclear staining to show cell locations was performed using DAPI (4′,6-diamidino-2-phenylindole) (blue), with neurons (and associated outgrowths) stained using a β-III tubulin fluorescent antibody (green), whilst magnetic nanoparticles (MNPs) could be observed due to their conjugation to a rhodamine fluorescent dye (red). Scale bars = 20 μm.

We therefore focused on a more detailed characterisation of the neurite orientation and corresponding magnetic force vectors for these dense cellular areas (shown as the dashed orange line in Scheme 1).

To validate and quantify the extent of neurite orientation, an analysis method was developed using the two-dimensional (2D) Fourier transform (FT) of the fluorescence images of neurites obtained from β-III tubulin staining. The 2D-FT converts the spatial intensity of an image to a 2D intensity plot in frequency space, thus providing information on spatial scales and texture within the image. Whilst isotropic variations in image features produce a circular distribution of intensity in the 2D-FT, anisotropy within an image will confine the intensity in the 2D-FT along specific directions. For example, an image composed of perfectly parallel lines would produce a 2D-FT with intensity concentrated along an axis orthogonal to the lines in the image. However, variations from this perfect alignment would produce a distribution in intensity about an axis orthogonal to the average orientation of the lines. This tool is therefore very useful for detecting texture within an image and has been used previously for both biological [40] and materials applications [41]. To determine the average orientation of neurites within the images here, we obtained the 2D-FT and then performed radial sums of the intensity measured outwards from the central point, as a function of angle. The peaks in these radial sum plots reveal the direction of an axis orthogonal to the average neurite fibre orientation, which is crossed twice during the full 360-degree radial sum.

For cells grown in the absence of a magnetic field (Fig. 3a), the corresponding 2D-FT displays a circular (symmetric) distribution of intensity about the central point (Fig. 3b). This is characteristic of a randomly orientated texture within the image (in this case the image texture being dominated by the neurites). To further quantify this, radial sums of the intensity within the 2D-FT were plotted as a function of angle (Fig. 3c). To provide comparisons between different images, the intensity shown in these plots was normalised to the total integrated intensity in the 2D-FT.

The same processes were performed on the fluorescence image taken from MNP loaded cells grown under magnetic field exposure (Fig. 3d-f). The orientation of the neurites seen in the fluorescence image (Fig. 3d) produces a distinct anisotropy of the intensity in the 2D-FT (resembling a bow tie in shape), along an axis that is perpendicular to the average orientation direction of the neurites (Fig. 3e). This anisotropy axis is revealed more clearly in the radial sum plot (Fig. 3f), showing two clear peaks separated by 180° that reveal the maximum intensity axis as the radial sum performs a complete revolution of 360°. From this analysis, the average neurite orientation is determined to be 25° with respect to the horizontal, which is consistent with a qualitative visualisation of the fluorescence image (Fig. 3d). In comparison, for the control sample only very weak peaks can be discerned at 0 and 180°, arising from an artefact producing weak horizontal and vertical intensity in the 2D-FT due to the image pixilation. In addition, small but sharp peaks can also be seen in the radial sum plots, and as streaks in the 2D-FTs indicating that a minor proportion of neurites within the images are preferentially orientated along other directions.

To assess the degree of correspondence between the magnetic forces imparted on the magnetic endosomes in the cells and the resulting orientation of the neurites, the direction and amplitude of the magnetic forces were determined by measuring the magnetic field distribution across the regions of cell growth. As described in the Experimental section, from these field measurements, the X, Y and Z components of the 3D field gradient were determined, and consequently the position-dependent magnetic field intensity gradient within the cell monolayer plane was obtained. The corresponding 3D force vector on a magnetic particle where the gradient magnetic field at the particle position is ∇H, and it is assumed that the particle moment is aligned with the local

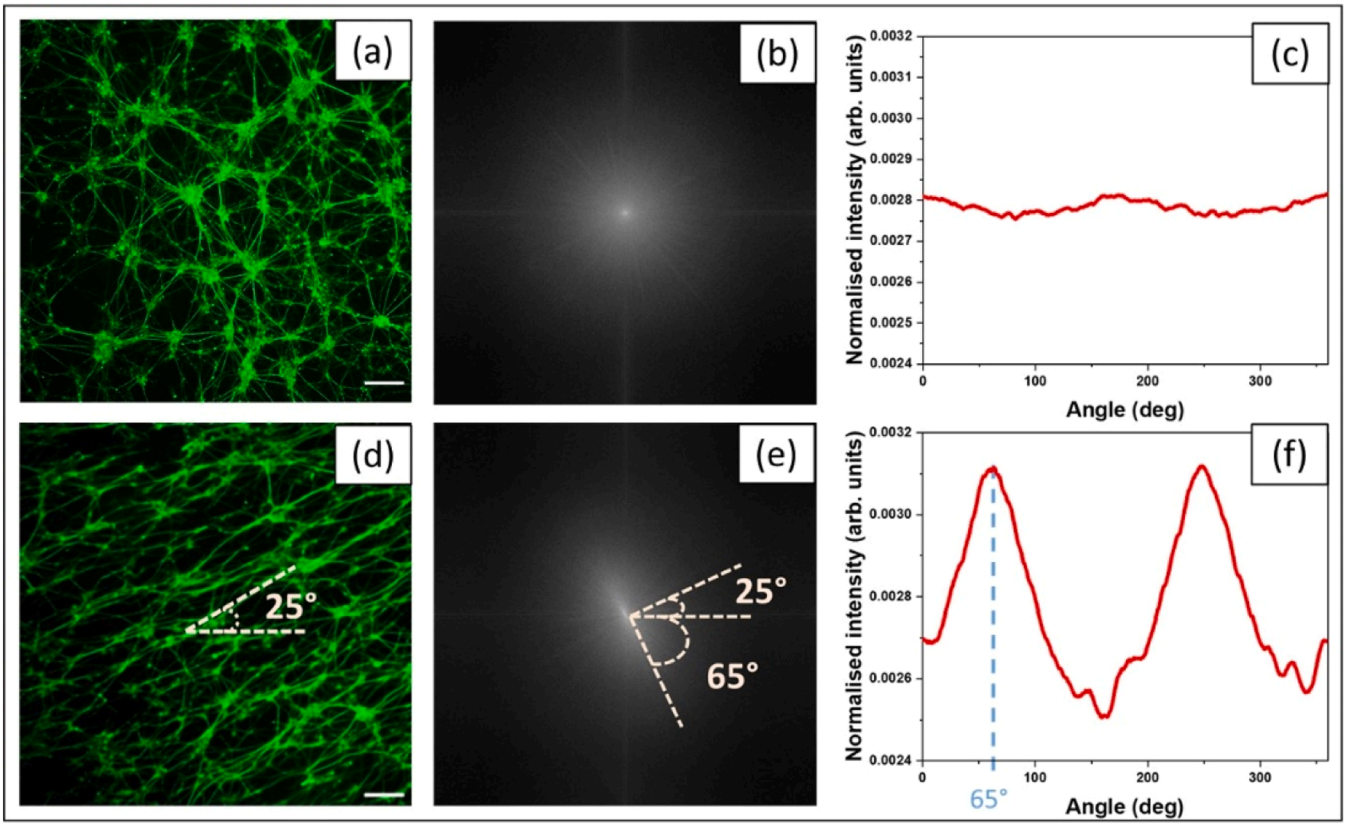

Fig. 3. Quantification of neurite orientation in fluorescence images of SH-SY5Y cells stained for β-III tubulin (a,d) using 2D FT of the fluorescence images (b,e) and corresponding radial sum plots (c,f). Analysis was performed on unloaded controls in the absence of a magnetic field (top row) and on MNP loaded cells grown under magnetic field exposure (bottom row). The intensity shown in the radial sum plots was normalised to the total integrated intensity in the 2D-FT. Scale bars = 100 μm.

magnetic field, is given by the expression:

$$\boldsymbol{F}_p = \mu_0 m_p \nabla H \tag{1}$$

where μ_0 is the permeability of free space, and m_p is the magnetic moment of the particle, *i.e.*

$$m_p = \rho V_p M_S \times 10^{-3} \tag{2}$$

with ρ being the mass density of the particles, V_p the particle volume, M_S the saturation magnetisation of the particles (in emu/kg), and the 10^{-3} term is required to convert from cgs to SI units.

For superparamagnetic particles, as used in the experiments here, in the absence of a magnetic field the directions of particle magnetic moments are constantly flipped due to thermal effects, resulting in a net zero magnetisation. However, when a field is applied a net magnetisation occurs that depends on the strength of the field and the temperature of the system. A Langevin function can be employed as a good approximation of this field dependent magnetisation behaviour. Thus, if the average number of superparamagnetic particles internalised within an endosome is given by N_{part}, then the force per endosome can be determined by scaling Eq. (1), modified to account for the use of superparamagnetic particles accordingly as:

$$\boldsymbol{F}_{endo} = N_{part} \times \mu_0 m_p \left\{ \coth(\varepsilon) - \frac{1}{\varepsilon} \right\} \nabla H \tag{3}$$

where the variable, ε, used in the Langevin function shown in the { } above is given by

$$\varepsilon = \frac{\mu_0 H m_p}{k_B T} \tag{4}$$

with k_B the Boltzmann constant, and T the temperature of the system.

The parameter N_{part} was obtained here from the earlier estimates of particle numbers in the endosomes derived from the TEM measurements (Figure S2, table S1), and this value and the other parameters required to determine the force vector in Eq. (3), are given in Figure S3 and table S2. An example of the field measurements across a region of interest on the magnet array plate corresponding to the height at which the cells were grown (*i.e.*, the cell monolayer), together with the derived force vectors, are shown in Fig. 4. The vertical component of the magnetic field depends on the position and orientation of the stacks, as well as the number of magnet discs in each stack (Fig. 4a), measured across the region of

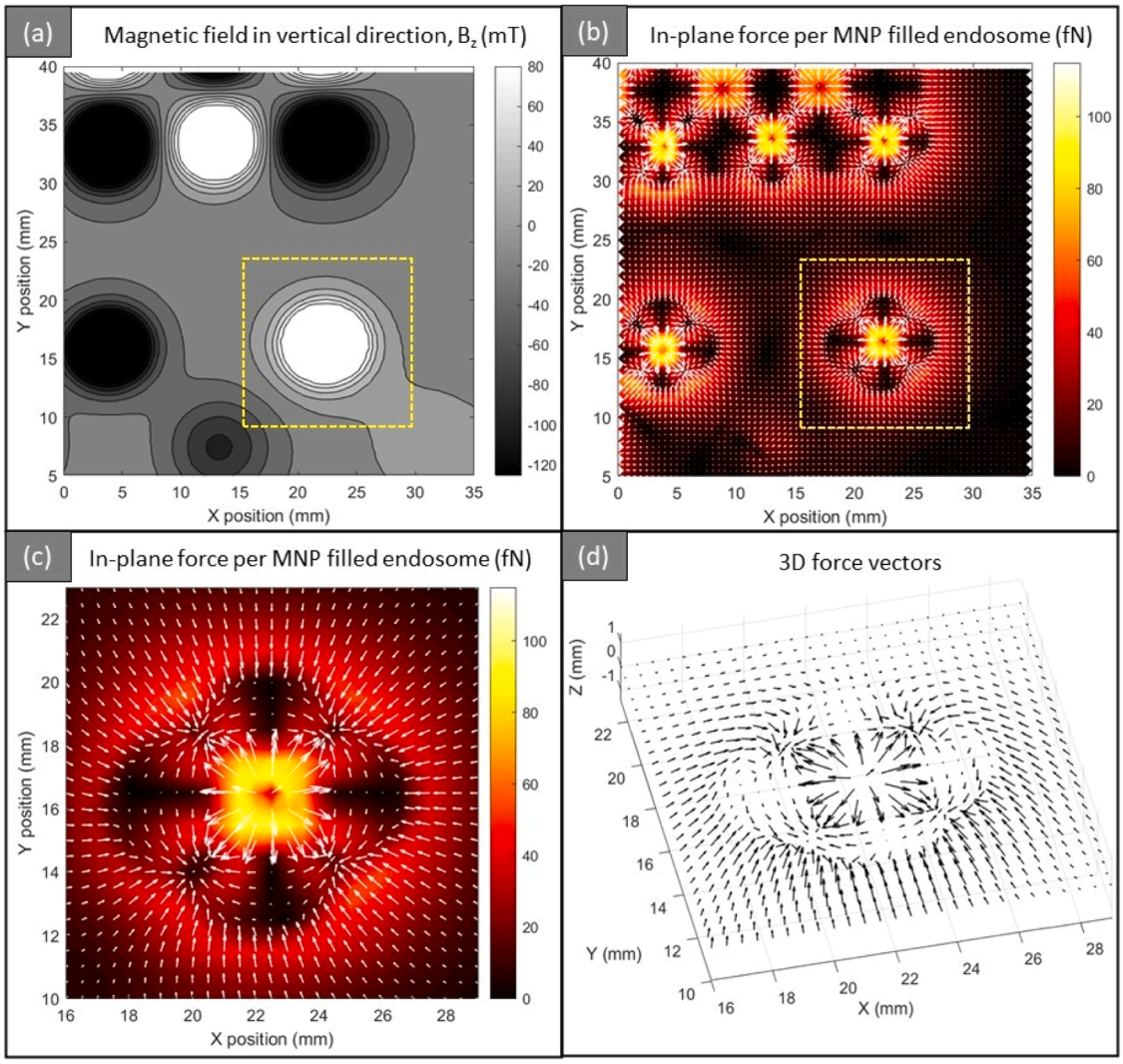

Fig. 4. Measurement and derivation of magnetic forces on magnetic nanoparticle clusters within cellular endosomes induced using the permanent magnet array plate. (a) The vertical component of the field across a region of interest, measured at the height of the cell monolayer. (b) Component of the magnetic forces in the cell monolayer plane, derived from spatially dependent magnetic field intensity measurements. (c) Enlarged region showing in-plane magnetic forces (yellow-boxed area in (b)). (d) 3D force vectors determined across the same area as shown in (c). The heat maps and associated colour bars in (b) and (c) indicate the magnitude of the in-plane force per nanoparticle filled endosome in fN.

interest. As the cells were grown under 2D cell culture conditions, the components of the forces within the cell monolayer plane are expected to dominate neurite outgrowth. These are shown in Figs. 4b and 4c, where the colour intensity is the amplitude of the in-plane force, and the arrows show the directions of these forces. As expected, the strongest forces occur in the vicinity of the magnet disc stacks, but the distribution of the forces shows complex behaviour that depends on the arrangement of neighbouring stacks.

An area corresponding to a region of interest where confluent cells were found directly above one of the magnet stacks in a follow up cell culture experiment is shown in Figs. 4c and 4d. Here, strong in-plane forces are directed outwards from the centre of the magnet disc towards the perimeter, which are met by weaker but more uniform forces directed towards the magnet from outside the perimeter. Closer inspection of the forces (Fig. 4c) reveals a slight asymmetry to the force distribution, caused by a neighbouring magnet stack positioned below and to the left. This asymmetry results in the angles of the in-plane force vectors that occur outside the magnet perimeter, to be greater (*i.e.*, aligned closer to the Y-axis) on the left-hand side of the region compared to those on the right. Analysis of the 3D force vectors (Fig. 4d) shows that the moderate force vectors in the outer region beyond the magnet perimeter are in fact tilted out of the cell plane, whilst the strong force vectors in the central region are fully in-plane. Strong vertical (out-of-plane) forces were found between these two regions, just outside the position of the magnetic rim (these can be seen more clearly in the animated 3D force vectors plots linked in the Supporting Information).

To compare the derived force vectors with the neuronal outgrowth observed, a set of low magnification fluorescence images were combined to obtain an area covering ~1cm^2, that was centred directly above the magnet stack discussed above during cell culture. The neurite orientation analysis presented earlier was employed to quantify the average alignment of neurite growth in the region just outside the magnet perimeter, where clear orientation could be observed (Figure S4). The resulting large area fluorescence map including this analysis is compared to the equivalent region of the in-plane magnetic force map in Fig. 5. It is immediately apparent from the figure that the orientation of the neurites in the outer regions, closely match the directions of the in-plane force vectors. This confirms that the neurite alignment observed in these regions, was indeed induced by the in-plane magnetic forces. Further conviction in this conclusion is given by the observation of left to right asymmetry in the distribution of the neurite orientation that is duplicated in the asymmetry seen in the force vectors, described above. However, some regions analysed in Fig. 5 do not match the force vectors quite as closely as others, perhaps indicating that alignment of neurites will also be affected by cellular growth in neighbouring regions.

As shown in Fig. 5, it appears that neurite alignment occurs when regions of parallel forces of moderate strength (*i.e.*, in-plane component of ~10–50 fN per magnetic endosome) are sustained over distances of several millimetres. This is consistent with previous suggestions that magnetic forces provide the necessary stimuli to sustain enhanced axon outgrowth [33], but in the case shown here, this is achieved over the much greater distances defined by the range of the aligning forces. Interestingly, the stronger (~100 fN per endosome) and purely in-plane forces found in the central region, do not appear to direct the neurite growth in the same way. Closer inspection of the inner-perimeter region where such strong in-plane forces converge (for example the dashed blue box shown in Fig. 5) revealed a dramatic impact on the resulting cell growth. The observed morphology of cells in these regions is strikingly different to the control (Fig. 6a). Although both groups show apparently random neurite orientation, the cells that were grown under magnetic field exposure in regions where the magnetic forces converge, have unusually thick neurite outgrowth forming straight connections between the much larger and denser neuroclusters observed. These large neuroclusters appear also to be heavily loaded with MNPs. However, unloaded cells found within the same region exhibit similar morphology and outgrowth to that of the control (see for example the "+ Field - MNP" control in Fig. 6b) and also (the "- Field + MNP" control shown in Fig. 1).

It seems therefore that the strong in-plane forces in these regions encourage the growth of large neuroclusters. This could be due to migration or possibly proliferation of MNP-loaded cells caused by the strong magnetic forces present. However, neuronal cells tend not to divide once differentiated, and even if the field did induce proliferation, a reduction in MNP loading of the cells would be expected due to cell division. In contrast, the resulting neuroclusters formed appear to be heavily loaded with MNPs, despite being >100 μm in diameter.

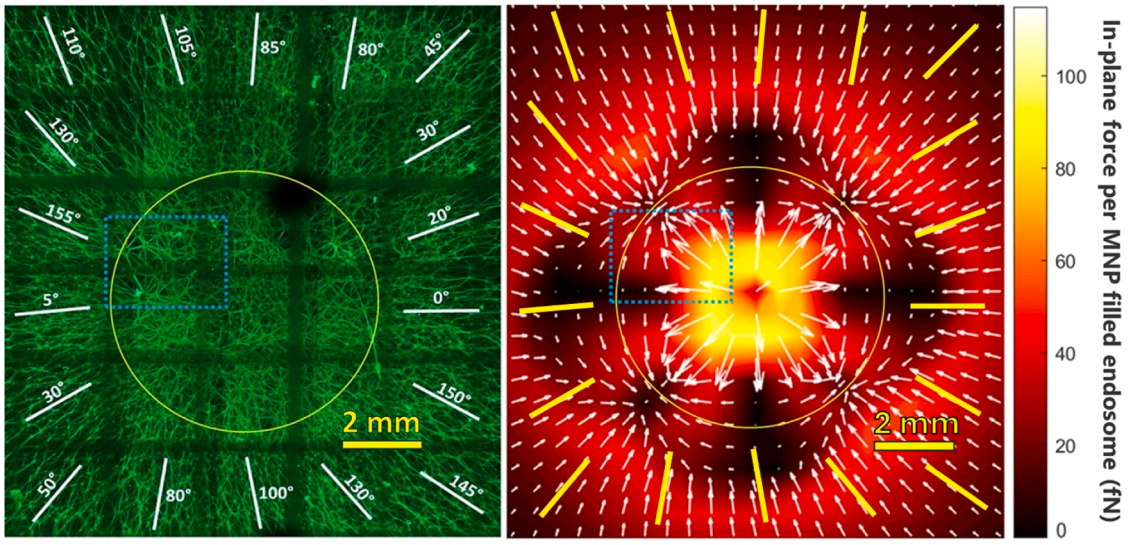

Fig. 5. Mapping of fibre growth compared to in-plane magnetic force vectors over a wide area of the culture (~1 cm^2). SH-SY5Y cells were stained for β-III tubulin showing average neurite orientation quantified using the 2D-FT method (LHS), compared to the in-plane magnetic forces determined for the same area (RHS). The average neurite orientations are overlaid as yellow lines on the magnetic force vector plot (RHS). The yellow circle represents the edge of the permanent magnet disc directly beneath the cell monolayer, and the dashed blue box is the region of interest shown in Fig. 6. The radial region just inside the yellow circle (that includes the dashed blue box) is referred to as the inner-perimeter region in the discussion, whilst the area where neurite orientation has been quantified is referred to as the outer-perimeter region. The dark gridlines seen in the composite fluorescence image (LHS) come from a detachable cell counting grid that was used to locate cell imaging positions relative to the magnet array.

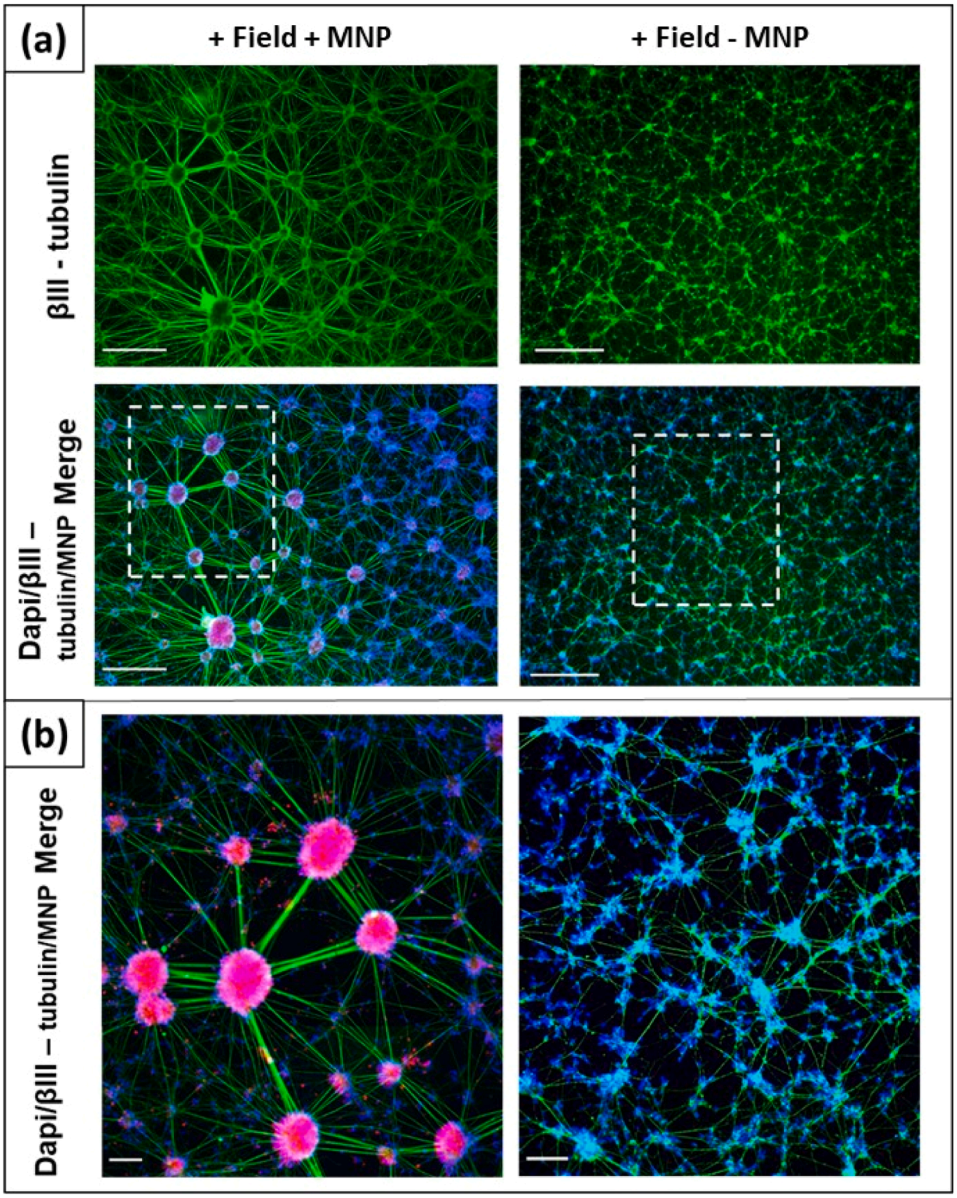

Fig. 6. Fluorescence images from SH-SY5Y cells with nuclear staining performed using DAPI (4′,6-diamidino-2-phenylindole) [blue], neurons (and associated outgrowths) stained using a β-III tubulin fluorescent antibody [green], and fluorescently tagged magnetic nanoparticles (MNPs) [red]. Cells were grown under magnetic field exposure with MNP loaded cells shown in the LH column, and unloaded cells shown in the RH column. (a) The region shown is identified by the dashed blue box in Fig. 5 (bottom row). Scale bars = 500 μm. (b) Higher magnification image of the region shown in the white dashed box in (a). Scale bar = 100 μm.

The formation of neuroclusters of SH-SY5Y cells appears to be ubiquitous in regions of high cell density. Figure S5 shows a comparison of cluster and neurite growth in cells under different magnetic field exposure and nanoparticle loading conditions. Small neuroclusters of variable sizes can be seen to form in all the control samples (Figure S5 a-c). However, for cells loaded with nanoparticles it is possible that the formation of clusters could be aided by cell migration influenced by the magnetic forces. Where no clear overall directionality to the magnetic force directions induced by the magnet array exists (as for the magnet centre (Figure S5(e)) and inner-perimeter (Figure S5 (f) regions), neurite growth appears to be dominated by nearest neighbour interactions between the clusters. This results in straight-line growth between clusters, as can be seen in the region directly above the magnet centre (Figure S5 (e)). It is possible that this straight-line growth is enhanced by the magnetic loading of these clusters, which will be magnetically polarized by the magnetic field, resulting in additional directional magnetic forces towards the clusters. This localised magnetic force could act on magnetically loaded cells, in a manner analogous to that observed by our group in our earlier work [24]. In this earlier study, an array of synthetic magnetically polarized pillars of a similar size to the larger magnetically loaded cell clusters observed here, were used to induce such local forces. However, the forces directed towards cell clusters are likely to be substantially weaker than those exerted by the pillars, due to the different magnetic field configurations and materials. Regardless of this, larger cell clusters (such as observed in Figure S5(f)) will produce proportionally stronger magnetic forces.

Where magnetic forces induced by the magnet array have clear long-range directionality (for example in the outer-perimeter region of the magnet, Figure S5(d)), the growth of neurites appears to be dominated by these forces as can be seen by the comparison of these magnetic force vectors with the neurite alignment (Fig. 5). Importantly, this effect was observed regardless of variations in local cell density or cluster formation (see for example Figs. 8, S1 and S7). Thus, the directional growth of neurites under these magnetic forces appears to be a fundamental effect

that does not rely on cluster formation, cell migration or proliferation. However, although these factors may not be prerequisites for alignment, it is possible that neurite growth is also influenced by them.

At the inner-perimeter region of the magnet, the magnetic force vectors converge. Thus, any mobile magnetically loaded cells would be focused into this region by the magnetic forces from the magnet array, which could account for the growth of the considerably large neuro-clusters observed in this region (Fig. 6, Figure S5(f)). The combined localisation of metabolically active cells in these large clusters, together with possible additional magnetic forces that are generated towards each neurocluster, could explain the thicker and straighter neurites observed in these regions. If sizeable local magnetic forces were to occur near these large magnetic neuroclusters, then magnetic endosomes within the growing neurites would be pulled towards the clusters at either end, potentially placing these growing neurites under mechanical tension.

The concept of tension-driven axon assembly has been reviewed previously in the context of mechanisms that accommodate the mass addition required for axons to elongate [42]. However, in our case both ends of the neurites are most-likely fixed in space, either by anchoring of the neuroclusters to the base of the cell culture well, or as a consequence of the dense cellular networks that are formed. In the absence of elongation, it may therefore be possible that the mass addition manifests as a thickening of the neurites formed between the neuroclusters. We have not yet assessed the mechanical and functional properties of these thick neurites. However, previous studies have shown that both structural and functional properties are preserved when axons are elongated under mechanical tension [43–45]. It is therefore possible that these thicker neurites could have enhanced structural and functional integrity compared to those formed naturally. It may be possible to evaluate such mechanical changes to neuronal cellular structures using techniques such as atomic force microscopy (AFM). A review of such methods can be found in the paper by Jembrek et al. [46].

In addition to tension induced responses, mechanical forces also control the gating of mechanosensitive channels such as Piezo, TRPV and TREK, which results in ion flux across the cell membrane. The downstream signalling events, triggered in response to ion flux, can regulate neuronal cell behaviours such as neurite extension and axon growth [31,47,48]. In the current study the local magnetic forces generated could therefore also be affecting the gating of mechano-sensitive channels at the cell membrane, resulting in the co-ordinated axon growth that is observed. These results align with previous work in this area which demonstrated the role of mechanosensitive channels in controlling neuron behaviour and axon growth [49].

In order to better understand how the magnetic forces induced the observed morphological changes to the cells, we explored changes to the functional signalling and metabolic pathways at the cellular level. To do this we employed bioinformatics analysis of proteomics data obtained by Sequential Window Acquisition of all Theoretical mass spectra (SWATH-MS). Using this approach, changes in protein expression in SH-SY5Y cells taken from experimental groups using an identical setup to the magnetic force exposed cells above, were compared to control cell groups grown with neither MNPs nor magnetic field exposure. In both cases the proteins were extracted from cells 3-weeks after MNP loading. In total, 10,982 proteins were identified. Following filtering to include only proteins identified from $\geq$2 peptides, the experimental and control groups were compared. Proteins that were statistically significant (p-value $\leq$0.01) with an expression change of at least 25 % included 134 proteins with reduced expression and 94 proteins with increased expression.

Table 1 summarises the molecules (*i.e.*, proteins) that were found to have $a \geq 50$ % change in expression in cells grown under magnetic force conditions compared to the control, and the corresponding cellular functions mapped to each set of proteins as identified by Ingenuity Pathway Analysis (IPA). The corresponding summary of molecules with a change in expression of $\geq$25 % is presented in table 2. The IPA analysis indicates functions that are statistically likely (p-value <0.01) to have been affected by the uptake of MNPs and/or application of magnetic forces to the cells.

From table 1, a statistically significant *activation* (magnitude of z-score $\geq$ 2) is seen for three functions, all of which are implicated in carbohydrate metabolism. Corresponding network diagrams derived from the analysis, showing an overview of all the affected functions associated with carbohydrate metabolism in table 1, are shown in Figure S6. The proteins DKK1 and sFRP1 are both implicated in Wnt signalling - a developmental pathway which is involved in the regulation of neuronal proliferation and differentiation[4]. The upregulation of these proteins indicated by the analysis (Table 1, Figure S6) would be expected to block Wnt signalling which could indirectly impact cellular metabolism [50].

Both the increase in carbohydrate metabolism and the anticipated downregulation of Wnt signalling could be associated with the uptake and subsequent processing of the MNPs by the cells. To investigate this further we performed an assay to study metabolic rate in cells at different time points following loading of cells with differing MNP concentrations, but without subsequent exposure to the magnetic field (Fig. 7). At day 3 the metabolic activity was found to increase in an approximately linear fashion as a function of MNP loading concentration (Fig. 7a) showing an almost 4-fold increase at the highest MNP concentration used compared to unloaded cells. However, 3 weeks after

Table 1
Molecule (protein) sets and associated cellular functions identified by Ingenuity Pathway Analysis (IPA) following mass spectrometry analysis of proteins extracted from cells. Data is shown for protein expression changed by 50 % or more in comparison to the control ($n = 3$), for SH-SY5Y cells loaded with MNPs and exposed to magnetic fields using identical processes to those used for the cells in Figs. 1–6. The p-value reflects the probability that the association of the biological function with the identified protein set could be attributable to chance alone ($p \geq 0.01$). The activation z-score indicates whether the function associated with a particular protein set is likely to be activated (positive score) or inhibited (negative score), with z-score magnitudes of ≥ 2 indicating statistically significant activation/inhibition. Where a z-score is not presented this indicates the effect was not predicted by the analysis. Official gene symbols are used to denote proteins (molecules).

Categories	Diseases or Functions Annotation	p-value	Activation z-score	Molecules
Carbohydrate metabolism	Metabolism of polysaccharide	0.000123	2.236	B4GALT7,DKK1,HGSNAT,LUM,PHKA1,PLIN2,PXYLP1,SFRP1,STBD1
	Metabolism of carbohydrate	0.000201	1.89	B4GALT7,DKK1,GAL,GALM,HGSNAT,LUM,MTMR14,PHKA1,PIK3R3,PLCG2,PLIN2, PML,PXYLP1,SFRP1,ST6GALNAC5,STBD1
	Synthesis of carbohydrate	0.000879	2.449	B4GALT7,DKK1,GAL,LUM,MTMR14,PHKA1,PIK3R3,PLCG2,PLIN2,PXYLP1,SFRP1, ST6GALNAC5
	Synthesis of glycosaminoglycan	0.00126	*not predicted*	B4GALT7,DKK1,LUM,PXYLP1,SFRP1
	Synthesis of polysaccharide	0.00308	2.236	B4GALT7,DKK1,LUM,PLIN2,PXYLP1,SFRP1
Small molecule biochemistry	Release of dopamine	0.00689	*not predicted*	CARTPT,CHRNA5,GAL
Cell morphology	Sprouting	0.0195	−0.896	ADAMTS1,CYLD,EIF4EBP1,MID1,PROX1,PRSS12,SEMA3C,TIMP3

Table 2
Molecule (protein) sets and associated cellular functions identified by Ingenuity Pathway Analysis (IPA) following mass spectrometry analysis of proteins extracted from cells. Data is shown for protein expression changed by 25 % or more in comparison to the control ($n = 3$), for SH-SY5Y cells loaded with MNPs and exposed to magnetic fields using identical processes to those used for the cells in Figs. 1–6. The p-value reflects the probability that the association of the biological function with the identified protein set could be attributable to chance alone ($p \geq 0.01$). The activation z-score indicates whether the function associated with a particular protein set is likely to be activated (positive score) or inhibited (negative score), with z-score magnitudes of ≥ 2 indicating statistically significant activation/inhibition. Where a z-score is not presented this indicates the effect was not predicted by the analysis. Official gene symbols are used to denote proteins (molecules).

Categories	Diseases or Functions Annotation	p-value	Activation z-score	Molecules
Cellular development	Growth of neurites	0.000117	1.05	CD47,DHCR24,EIF4EBP1,EXTL3,FGF1,GAL,GNAQ,MDK,MFN1,MID1,NDEL1,PRPH,RPL4, SEMA3C,VIM,VPS13B,ZFYVE26
	Outgrowth of neurites	0.00107	1.528	CD47,EXTL3,FGF1,GAL,GNAQ,MDK,MFN1,NDEL1,PRPH,RPL4,VIM,VPS13B,ZFYVE26
	Proliferation of neuronal cells	0.000104	1.44	CD47,DHCR24,EIF4EBP1,EXTL3,FGF1,GAL,GNAQ,IGFBP2,MDK,MFN1,MID1,NDEL1,PRPH, RPL4,SEMA3C,VIM,VPS13B,ZFYVE26,ZNF335
Cellular assembly and organisation	Movement of lysosome	0.00263	*not predicted*	MYO1B,NDEL1
	Organization of cytoplasm	0.00312	1.002	ANPEP,CD47,CEP192,CEP72,CYLD,DKK1,EIF4EBP1,FGF1,FHL2,FMNL2,GAL,LDLR,MDK, MFN1,MID1,MKLN1,MPP1,MRTFA,MYO1A,MYO1B,NCKIPSD,NDEL1,PEX2,PLCG2,PRPH, PRSS12,PTCD2,RPL4,SEMA3C,SFRP1,SLC3A2,TIMP3,TRAPPC8,VIM,WDR81,ZNF335
	Organization of cytoskeleton	0.00716	1.002	ANPEP,CD47,CEP192,CEP72,CYLD,DKK1,EIF4EBP1,FGF1,FHL2,FMNL2,GAL,LDLR,MDK, MFN1,MID1,MKLN1,MPP1,MRTFA,MYO1A,MYO1B,NCKIPSD,NDEL1,PLCG2,PRPH,PRSS12, RPL4,SEMA3C,SFRP1,SLC3A2,TIMP3,VIM,ZNF335
Cellular growth and proliferation	Growth of neurites	0.000117	1.05	CD47,DHCR24,EIF4EBP1,EXTL3,FGF1,GAL,GNAQ,MDK,MFN1,MID1,NDEL1,PRPH,RPL4, SEMA3C,VIM,VPS13B,ZFYVE26
	Outgrowth of neurites	0.00107	1.528	CD47,EXTL3,FGF1,GAL,GNAQ,MDK,MFN1,NDEL1,PRPH,RPL4,VIM,VPS13B,ZFYVE26
	Proliferation of neuronal cells	0.000104	1.44	CD47,DHCR24,EIF4EBP1,EXTL3,FGF1,GAL,GNAQ,IGFBP2,MDK,MFN1,MID1,NDEL1,PRPH, RPL4,SEMA3C,VIM,VPS13B,ZFYVE26,ZNF335
Cell morphology	Elongation of cells	0.00559	*not predicted*	CD47,FGF1,MFN1,SFRP1

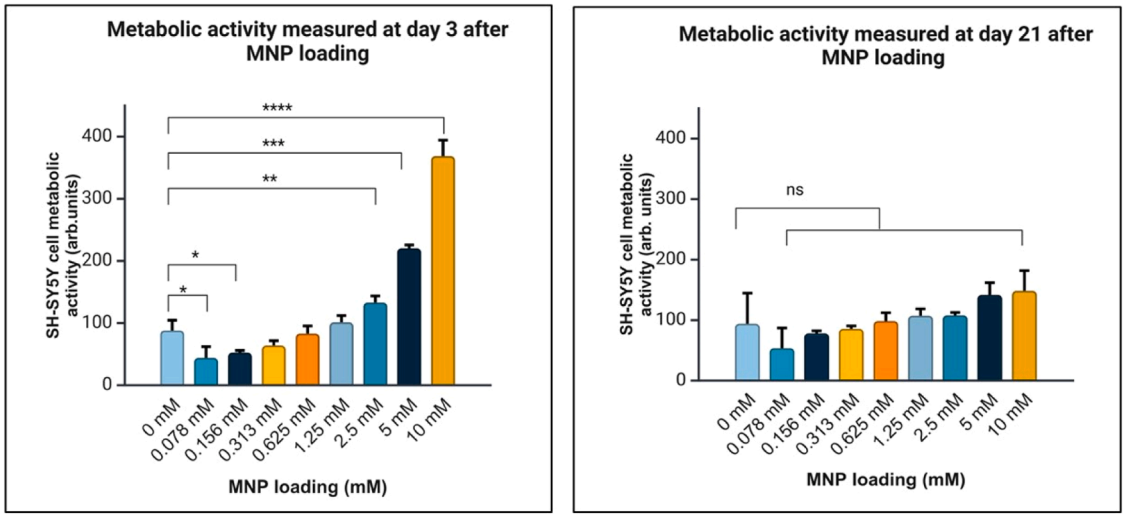

Fig. 7. Cell metabolic rate assessed using the colorimetric XTT assay (absorbance, OD 450 nm). SH-SY5Y cells were analysed following their loading with different MNP concentrations ($n = 4$). Results are shown on: (a) day 3 after MNP loading, and (b) day 21 after MNP loading. Error bars = SEM, * ($p < 0.05$), ns (no significance).

MNP loading the effect had diminished for even the highest MNP concentration (Fig. 7b). The transient nature of the effect suggests that it is unlikely that MNP loading of cells alone is responsible for the increase in carbohydrate metabolism found in the cells used in the proteomics experiment, as these were processed at the same late time point (3 weeks after MNP loading). It is therefore possible that the application of mechanical (magnetic) forces could also play a role in the enhanced metabolism of the cells.

In addition to changes to carbohydrate metabolism, alterations to functions associated with cellular growth and development were found when proteins with a change in expression of >25 % were included and analysed (table 2). From the table, an apparent trend in activation can be seen for functions associated with processes that enhance neurite development, such as cellular re-organisation and growth. Cellular re-organisation is known to involve the Wnt signalling pathway [51] and so the observed upregulation of the DKK1 protein which blocks this pathway, could also play a role here. In this case the magnitude of the activation z-scores was <2 and so it was not possible to assign statistical significance to the apparent activation of these functions. However, the consistently low p-values derived clearly indicate that these processes were affected by the uptake of MNPs and exposure to magnetic forces experienced by the cells.

As discussed earlier, in prior work [33] RNA sequencing of axons under magnetic stretching revealed cytoskeleton remodelling, which also features in the IPA analysis here (table 2). This previous study also found evidence of cellular processes that can modulate high energy metabolism, which could link to the increased carbohydrate metabolism described above. However, when making comparisons between these earlier measurements and the proteomics data reported here, it is necessary to account for the different targets in each case (axons in the prior study *versus* whole cell populations in the current work). In addition, proteomics and RNA sequencing would not necessarily be expected

to follow the same patterns, as the latter measures processes upstream of post-transcriptional regulation that affects protein expression [52].

From the experiments described above, induced orientation and changes in neurite outgrowth and morphology are seen to occur after 2–3 weeks of cell culture under the influence of magnetic forces. To develop further insight into the onset of directional neurite outgrowth, we conducted a study to assess neuronal alignment of MNP loaded cells cultured on the magnet array plate at an earlier stage of growth. In agreement with our own observations, published differentiation protocols suggest that SH-SY5Y cells begin to project neurite outgrowth between day 7–10 [53]. Therefore, onset of neurite orientation was studied for cells exposed to magnetic forces for 3 days following MNP labelling (corresponding to days 8–10 post differentiation). These cells would thus experience magnetic forces during the early stages of neurite outgrowth, and were subsequently fixed and analysed 3 weeks after MNP labelling.

The resulting fluorescence images obtained are shown in Fig. 8, revealing a pronounced degree of orientation of the neurites after only 3 days of magnetic force exposure. This was quantified as before, using the 2D-FT analysis, with clear peaks being observed in the radial sum plot that are extremely similar to those measured from the equivalent 3-week exposure (Fig. 8). In particular, the orientation of the neurites appears to be identical at this early stage of growth to that found in the longer term sample. Although the density and morphology of the neurites in this 3-day sample is different to that in the longer-term sample, the cell confluence was much lower and so direct comparisons require caution. Owing to this low confluence, there were insufficient cells in the 3-day sample for clear observations in the regions where large neuroclusters were previously observed (Figure 6; Figure S5f). However, an assessment of the outer-perimeter regions revealed a remarkably close agreement to the neurite alignment found in the 3-week exposure sample (Figure S7). The development of induced neurite orientation after only 3 days of magnetic force exposure is likely to be enhanced by the stimulated metabolism of the cells at this time point due to MNP internalisation, as discussed earlier (Fig. 7).

In an additional experiment, we examined cells exposed to magnetic forces for just 3 h after MNP labelling. We anticipated that such a time scale would be too short for mechanically stimulated orientation effects to occur. However, free MNP clusters should respond very rapidly to the magnetic field gradients produced by the array, and so this process would align any MNPs that avoided both cellular capture and the subsequent washing steps that were applied prior to positioning on the magnet array. Alignment of such free MNP clusters on the well plate might provide topological guidance cues for neurite outgrowth that reflected the magnetic force vectors from the array but would not require sustained magnetic forces during neurite growth. However, no evidence of alignment was found when cells exposed to the magnetic array for 3 h were compared to those exposed for 3 days (Figure S8), confirming that the orientation effects observed were unlikely to be caused by such topological effects.

To confirm that the orientation effects observed in the SH-SY5Y cells were not unique to immortalised cells lines, we performed similar experiments with primary rat cortical neurons exposed to the magnet array during cell culture. As with the SH-SY5Y cells, we found uptake of MNPs occurred within a 48-hour period. TEM analysis performed on primary cells following MNP labelling revealed aggregation of MNPs within endosomes, in a similar fashion to that found with the SH-SY5Y cells (Figure S9). After 4 days of exposure to magnetic fields, the cells were fixed and stained as before. The resulting fluorescence images show a clear alignment of neuronal processes for the cells loaded with MNPS

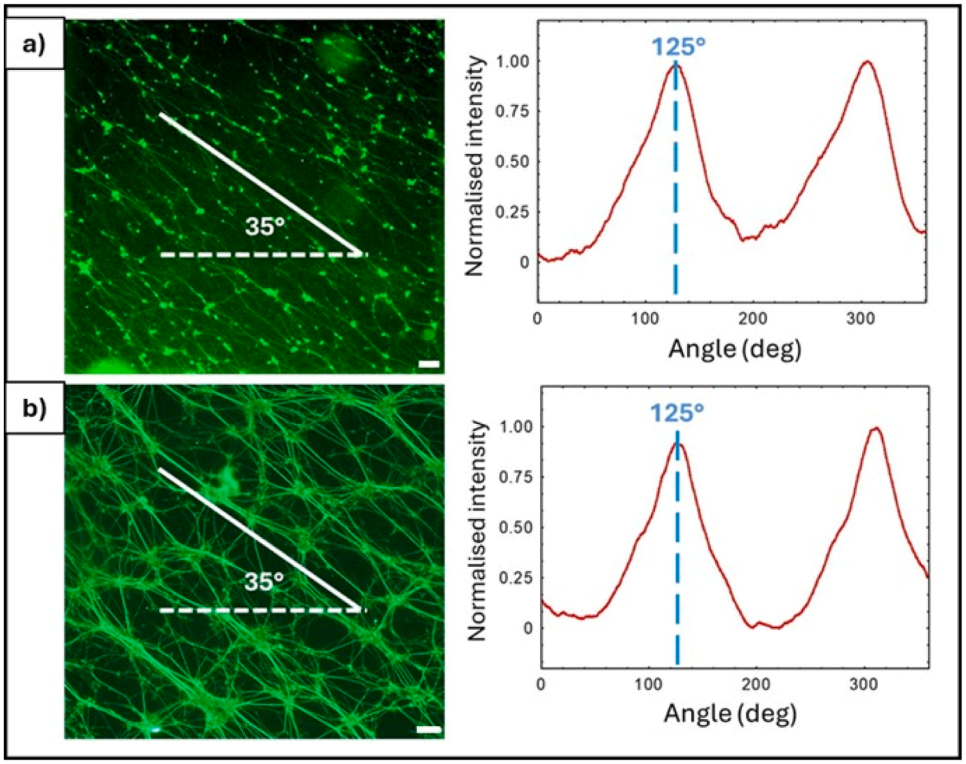

Fig. 8. Assessment of magnetic field exposure confined to early-stage neurite outgrowth vs longer term exposure, for cells grown in the same position on the magnet array. Imaging and analysis were performed 3 weeks after MNP labelling for both cases. (a) MNP loaded SH-SY5Y cells grown in a magnetic field for 3 days (days 8–10 post differentiation). (b) MNP loaded SH-SY5Y cells grown under magnetic field exposure for 3 weeks (days 8–28 post differentiation). Fluorescence images are shown (LHS) for neurons (and associated outgrowths) stained using a β-III tubulin fluorescent antibody [green] Radial sum plots obtained from the 2D-FT of the fluorescence images are shown for each sample (RHS). Given the variation in feature intensity in the two images, for a better comparison of the peak shapes and positions in the radial sum plots, a background intensity was removed from the data and the maximum intensity normalised to unity. The analysed regions in both cases correspond to box 15 in Figure S4. Scale bars = 100 μm.

and grown under magnetic field exposure (Fig. 9). In addition, we found that primary cells grown on the same magnet array arrangement used earlier (Fig. 5) were aligned along very similar directions to the SHSY-5Y cells, which also corresponded to the derived magnetic force vectors for the regions observed (Figure S10).

At this stage of culture for these primary cells, the formation of large clusters of primary neurons can be seen for all growth conditions, with evidence of MNP labelling of neurons (Fig. 9a). Additional observations of primary cells grown with and without MNP labelling and magnetic field exposure, are presented in Figure S11, and show similar clustering effects with clear localisation of MNPs into these large neuroclusters. However, the formation of thick, linear, and possibly multi-stranded fibres can only be observed for the cells containing MNPs and grown under a magnetic field (Fig. 9(b) and (c)), again suggesting the role of magnetic forces on driving the development of this morphology.

The ability to see magnetic force alignment effects in primary neuronal cells offers potential for exploring the control of axonal growth using *in vivo* models. Such studies would require more sophisticated methods to obtain the desired magnetic force vectors than the simple permanent magnet array systems applied here. One possibility would be to exploit magnetic field gradients similar to those used in magnetic particle imaging (MPI) instruments. An exploration of using the magnetic forces obtainable in such systems to guide magnetic particles has been described previously Griese et al. [54]. However, further development work will be necessary to accommodate the MNPs and field gradients needed for alignment of axons *in vivo*.

4. Conclusion

In summary, we have demonstrated the induction of long-range neurite orientation using magnetic forces as low as 10 fN acting on neuronal endosomes partially filled with MNPs. Using a simple system consisting of an aluminium plate holder enabling differing arrangements of stacks of cylindrical permanent magnets, we were able to create a variable magnetic force distribution over large areas where cells were grown in 2D culture. The alignment of the neurites in different regions of the cell culture was quantified using an analysis of the 2D-FT of the fluorescence images, following staining with a β-III tubulin fluorescent antibody. A detailed characterisation of the magnetic force vectors revealed a close correspondence with the average alignment of the neurites, confirming that the magnetic forces were able to guide neurite growth.

By subjecting the cells to extremely low forces over an extended growth period of several weeks, we have shown clear changes in orientation and cell morphology. This is in contrast to previous studies in which higher forces over a shorter period have resulted in less noticeable differences [24]. We have also demonstrated that directed neuronal alignment can be achieved over long distances using just magnetic forces, without the topographical or chemical cues required in previous work [29,30]. This is particularly significant for applications in neuroregeneration, as cells within the central nervous system may not exhibit the same topographical or chemical cues. A bioinformatics analysis of protein expression in cells exposed to magnetic forces, indicated an activation of carbohydrate metabolism, with further evidence suggesting processes related to cellular organisation were also affected.

In addition to the alignment of neurites, we also found that strong in-

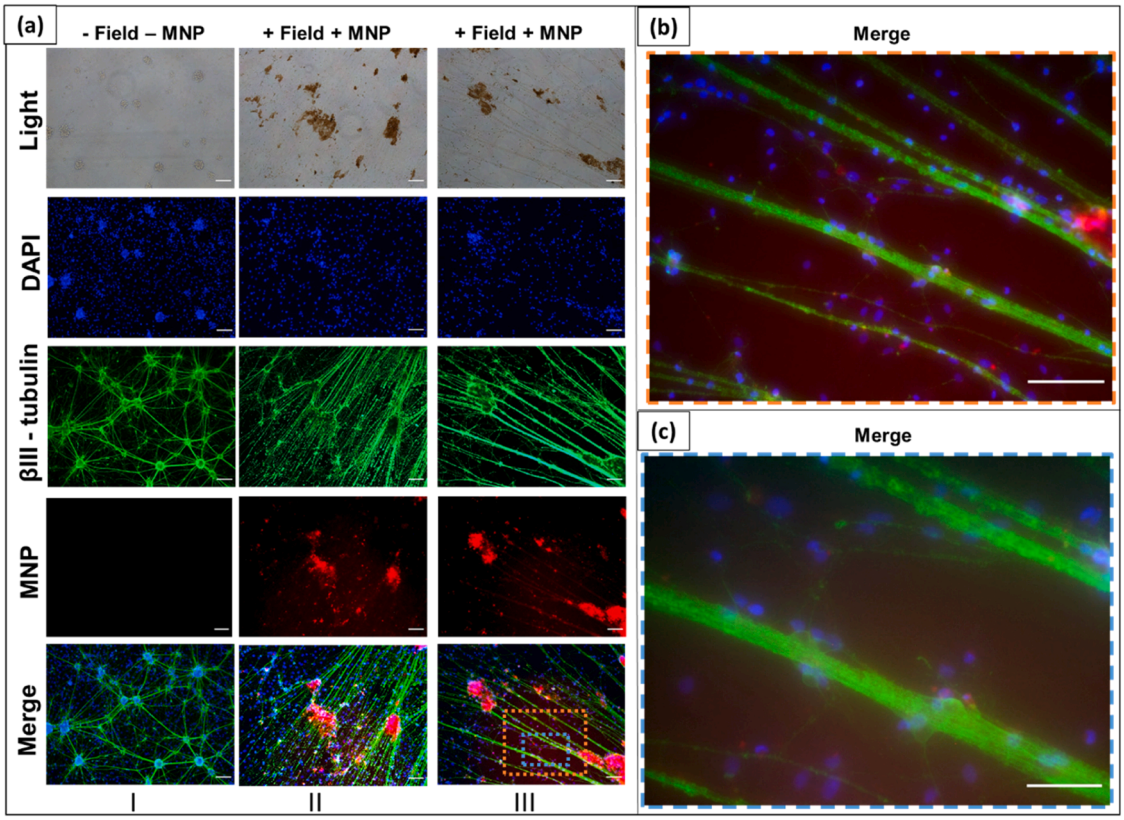

Fig. 9. Bright field (first row) and fluorescence microscopy images of primary rat cortical neurons cultured under different magnetic field exposure conditions for 4 days and subsequently fixed 7 days post culture. Nuclear staining to show cell locations was performed using DAPI (4′,6-diamidino-2-phenylindole) [blue], with neurons (and associated outgrowths) stained using a β-III tubulin fluorescent antibody [green], whilst magnetic nanoparticles (MNPs) could be observed due to their conjugation to a rhodamine fluorescent dye [red]. For part (a) Controls are shown in the first column whilst the second and third columns show cells grown in different positions on a magnet array. Parts (b) and (c) depicts higher magnification of the areas indicated by the orange and blue dashed squares in (a). Scale bar = 100μ m for part (a) and (b) and 50μ m for part c.

plane forces could dramatically enhance the growth of cellular neuroclusters in differentiating cells, as well as creating highly unusual thick linear neurite networks between them. We suggest that these large (~100 μm) MNP-loaded neuroclusters could function as localised magnetic particles. This could account for the neurite growth, as they would contribute additional magnetic forces directed along the shortest paths between the neuroclusters. To our knowledge, this type of cellular structure has not been witnessed before and could find applications in the creation of artificial neuronal networks, with the morphology of these thick linear neurites possibly enabling enhanced electrophysiological performance. However, the utilisation of MNP loaded cellular networks will also require assessment of exogenous MNP uptake on neuronal cell functional behaviour independently of magnetic force application, particularly in cases where large clustering of cells occurs. This could be achieved by studying protein and gene expression as a function of MNP loading and cell clustering, using similar methods to those applied here. In addition, the future development of more sophisticated magnetic field systems that allow independent control of both force amplitude and direction, will help determine the cellular mechanisms that dominate either axon reorganisation or growth. Such studies will inform on the potential efficacy of magnetic force-based methods for engineering neural circuitry.

CRediT authorship contribution statement

Tasmin Nahar: Writing – review & editing, Writing – original draft, Visualization, Validation, Software, Resources, Methodology, Investigation, Formal analysis, Data curation, Conceptualization. **Monte Gates:** Writing – review & editing, Writing – original draft, Supervision, Resources, Methodology, Investigation, Formal analysis, Data curation, Conceptualization. **Emilie Secret:** Writing – review & editing, Writing – original draft, Validation, Resources, Methodology, Investigation, Formal analysis, Data curation, Conceptualization. **Jean-Michel Siaugue:** Writing – review & editing, Writing – original draft, Resources, Methodology, Formal analysis, Data curation. **Jérôme Fresnais:** Writing – review & editing, Writing – original draft, Methodology, Investigation, Data curation, Conceptualization. **Michael Rotherham:** Writing – review & editing, Writing – original draft, Visualization, Validation, Supervision, Methodology, Investigation, Formal analysis, Data curation, Conceptualization. **Heidi R. Fuller:** Writing – review & editing, Writing – original draft, Methodology, Investigation, Formal analysis, Data curation. **Sharon J. Brown:** Writing – review & editing, Writing – original draft, Methodology, Investigation, Formal analysis, Data curation. **Alicia J. El Haj:** Writing – review & editing, Writing – original draft, Supervision, Methodology, Investigation, Funding acquisition, Data curation. **Neil D. Telling:** Writing – review & editing, Writing – original draft, Validation, Supervision, Resources, Project administration, Methodology, Investigation, Funding acquisition, Formal analysis, Data curation, Conceptualization.

Declaration of competing interest

The authors declare that they have no known competing financial interests or personal relationships that could have appeared to influence the work reported in this paper.

Acknowledgements

We would like to acknowledge Karen Walker for technical assistance. We acknowledge financial support from the European Union's Horizon 2020 Research and Innovation Programme under grant agreement No 686,841 (MAGNEURON). The authors also acknowledge the EPSRC for PhD studentship funding via the Centre for Doctoral Training (CDT) in Regenerative medicine (grant number: EP/L015072/1), as well as further EPSRC support under grant number EP/X014126/1. We would also like to acknowledge the support of Dr's Sally Shirran and Silvia Synowsky from the BSRC Mass Spectrometry and Proteomics Facility at the University of St Andrews.

Data availability

The raw and processed data required to reproduce these findings are available to download from the Keele Research Repository (http://doi.org/10.21252/d3fj-4m94).

Supplementary materials

Supplementary material associated with this article can be found, in the online version, at doi:10.1016/j.actbio.2024.12.057.

References

[1] G. DeMaagd, A. Philip, Parkinson's disease and its management: part 1: disease entity, risk factors, pathophysiology, clinical presentation, and diagnosis, Pharm. Ther. 40 (2015) 504.
[2] J. Dobson, Remote control of cellular behaviour with magnetic nanoparticles, Nat. Nanotechnol. 3 (2008) 139–143.
[3] C.C. Berry, A.S.G. Curtis, Functionalisation of magnetic nanoparticles for applications in biomedicine, J. Phys. D Appl. Phys. 36 (2003) R198.
[4] M. Rotherham, T. Nahar, T. Goodman, N. Telling, M. Gates, A. El Haj, Magnetic mechanoactivation of wnt signaling augments dopaminergic differentiation of neuronal cells, Adv. Biosys. 3 (2019) 1900091.
[5] J.H. Kordower, J.M. Rosenstein, T.J. Collier, M.A. Burke, E.Y. Chen, J.M. Li, L. Martel, A.E. Levey, E.J. Mufson, T.B. Freeman, C.W. Olanow, Functional fetal nigral grafts in a patient with Parkinson's disease: chemoanatomic, ultrastructural, and metabolic studies, J. Comp. Neurol. 370 (1996) 203–230.
[6] J.H. Kordower, T.B. Freeman, B.J. Snow, F.J. Vingerhoets, E.J. Mufson, P. R. Sanberg, R.A. Hauser, Smith, G.M. Nauert, D.P. Perl, Neuropathological evidence of graft survival and striatal reinnervation after the transplantation of fetal mesencephalic tissue in a patient with Parkinson's disease, N. Engl. J. Med. 332 (1995) 1118–1124.
[7] D.M. Suter, K.E. Miller, The emerging role of forces in axonal elongation, Prog. Neurobiol. 94 (2011) 91–101, https://doi.org/10.1016/j.pneurobio.2011.04.002.
[8] V. Raffa, Force: a messenger of axon outgrowth, Semin. Cell Dev. Biol. 140 (2023) 3–12, https://doi.org/10.1016/j.semcdb.2022.07.004.
[9] D.E. Koser, A.J. Thompson, S.K. Foster, A. Dwivedy, E.K. Pillai, G.K. Sheridan, H. Svoboda, M. Viana, L.D.F. Costa, J. Guck, C.E. Holt, K. Franze, Mechanosensing is critical for axon growth in the developing brain, Nat. Neurosci. 19 (2016) 1592–1598, https://doi.org/10.1038/nn.4394.
[10] M. O'Toole, P. Lamoureux, K.E. Miller, A physical model of axonal elongation: force, viscosity, and adhesions govern the mode of outgrowth, Biophys. J. 94 (2008) 2610–2620, https://doi.org/10.1529/biophysj.107.117424.
[11] K. Franze, J. Guck, The biophysics of neuronal growth, Reports Prog. Phys. 73 (2010) 094601.
[12] D.M. Suter, L.D. Errante, V. Belotserkovsky, P. Forscher, The Ig superfamily cell adhesion molecule, apCAM, mediates growth cone steering by substrate-cytoskeletal coupling, J. Cell Biol. 141 (1998) 227–240, https://doi.org/10.1083/jcb.141.1.227.
[13] D. Bray, Axonal growth in response to experimentally applied mechanical tension, Dev. Biol. 102 (1984) 379–389, https://doi.org/10.1016/0012-1606(84)90202-1.
[14] I.C.D. Lenton, E.K. Scott, H. Rubinsztein-Dunlop, I.A. Favre-Bulle, Optical tweezers exploring neuroscience, Front. Bioeng. Biotechnol. 8 (2020) 602797.
[15] D. Kilinc, A. Blasiak, J.J. O'Mahony, G.U. Lee, Low piconewton towing of CNS axons against diffusing and surface-bound repellents requires the inhibition of motor protein-associated pathways, Sci. Rep. 4 (2014) 7128.
[16] J.A. Abraham, C. Linnartz, G. Dreissen, R. Springer, S. Blaschke, M.A. Rueger, G. R. Fink, B. Hoffmann, R. Merkel, Directing Neuronal Outgrowth and Network Formation of Rat Cortical Neurons by Cyclic Substrate Stretch, Langmuir 35 (2019) 7423–7431, https://doi.org/10.1021/acs.langmuir.8b02003.
[17] M. Porta-de-la-Riva, A.C. Gonzalez, N. Sanfeliu-Cerdán, S. Karimi, N. Malaiwong, A. Pidde, L.F. Morales-Curiel, P. Fernandez, S. González-Bolívar, C. Hurth, M. Krieg, Neural engineering with photons as synaptic transmitters, Nat. Methods 20 (2023) 761–769, https://doi.org/10.1038/s41592-023-01836-9.
[18] D. Gothard, M. Rotherham, E.L. Smith, J.M. Kanczler, J. Henstock, J.A. Wells, C. A. Roberts, O. Qutachi, H. Peto, H. Rashidi, L. Rojo, L.J. White, M.M. Stevens, A. J. El Haj, F.R.A.J. Rose, R.O.C. Oreffo, *In vivo* analysis of hybrid hydrogels containing dual growth factor combinations, and skeletal stem cells under mechanical stimulation for bone repair, Mechanobiol. Med. 2 (2024) 100096, https://doi.org/10.1016/j.mbm.2024.100096.
[19] G.F. Goya, M.P. Calatayud, B. Sanz, M. Giannaccini, V. Raffa, T.E. Torres, M. R. Ibarra, Magnetic nanoparticles for magnetically guided therapies against neural diseases, MRS Bull. 39 (2014) 965–969.
[20] C.C. Hua, S. Zakaria, R. Farahiyan, L.T. Khong, K.L. Nguyen, M. Abdullah, S. Ahmad, Size-controlled synthesis and characterization of Fe3O4nanoparticles by chemical coprecipitation method, Sains Malays. 37 (2008) 389–394.
[21] H. Schöneborn, F. Raudzus, E. Secret, N. Otten, A. Michel, J. Fresnais, C. Ménager, J.M. Siaugue, H. Zaehres, I.D. Dietzel, R. Heumann, Novel tools towards magnetic

guidance of neurite growth: (I) guidance of magnetic nanoparticles into neurite extensions of induced human neurons and *in vitro* functionalization with Ras regulating proteins, J. Funct. Biomater. 10 (2019) 32, https://doi.org/10.3390/jfb10030032.

[22] M. Rotherham, T. Nahar, T.J. Broomhall, N.D. Telling, A.J. El Haj, Remote magnetic actuation of cell signalling for tissue engineering, Curr. Opin. Biomed. Eng. 24 (2022) 100410, https://doi.org/10.1016/j.cobme.2022.100410.

[23] F. Raudzus, H. Schöneborn, S. Neumann, E. Secret, A. Michel, J. Fresnais, O. Brylski, C. Ménager, J.M. Siaugue, R. Heumann, Magnetic spatiotemporal control of SOS1 coupled nanoparticles for guided neurite growth in dopaminergic single cells, Sci. Rep. 10 (2020) 1–15, https://doi.org/10.1038/s41598-020-80253-w.

[24] M. Bongaerts, K. Aizel, E. Secret, A. Jan, T. Nahar, F. Raudzus, S. Neumann, N. Telling, R. Heumann, J.M. Siaugue, C. Ménager, J. Fresnais, C. Villard, A. El Haj, J. Piehler, M.A. Gates, M. Coppey, Parallelized manipulation of adherent living cells by magnetic nanoparticles-mediated forces, Int. J. Mol. Sci. 21 (2020) 1–20, https://doi.org/10.3390/ijms21186560.

[25] J.M. Kanczler, H.S. Sura, J. Magnay, D. Green, R.O.C. Oreffo, J.P. Dobson, A.J. El Haj, Controlled differentiation of human bone marrow stromal cells using magnetic nanoparticle technology, Tissue Eng. Part A 16 (2010) 3241–3250, https://doi.org/10.1089/ten.tea.2009.0638.

[26] M. Puig-De-Morales, M. Grabulosa, J. Alcaraz, J. Mullol, G.N. Maksym, J. J Fredberg, D. Navajas, Measurement of cell microrheology by magnetic twisting cytometry with frequency domain demodulation, J. Appl. Physiol. 91 (2001) 1152–1159.

[27] A. Gahl, T.J. Kunze, Force-Mediating Magnetic Nanoparticles to Engineer Neuronal Cell Function, Front. Neurosci. 12 (2018) 299.

[28] R. Harrison, J. Luckett, S. Marsh, H.A. Lugo Leija, S. Salih, R. Alkharji, V. Sottile, Magnetically Assisted Control of Stem Cells Applied in 2D, 3D and In Situ Models of Cell Migration, Molecules 24 (2019) 1563.

[29] O. Antman-Passig, M. Shefi, Remote magnetic orientation of 3D collagen hydrogels for directed neuronal regeneration, Nano Lett 16 (2016) 2567–2573.

[30] Y. Jin, J.U. Lee, E. Chung, K. Yang, J. Kim, J.W. Kim, J.S. Lee, A.N. Cho, T. Oh, J. H. Lee, S. Cho, Magnetic Control of Axon Navigation in Reprogrammed Neurons, Nano Lett 19 (2019) 6517–6523.

[31] M. Rotherham, Y. Moradi, T. Nahar, D. Mosses, N. Telling, A.J. El Haj, Magnetic activation of TREK1 triggers stress signalling and regulates neuronal branching in SH-SY5Y cells, Front. Med. Technol. 4 (2022) 981421, https://doi.org/10.3389/fmedt.2022.981421.

[32] K. Dhillon, K. Aizel, T.J. Broomhall, E. Secret, T. Goodman, M. Rotherham, N. Telling, J.M. Siaugue, C. Ménager, J. Fresnais, M. Coppey, A.J. El Haj, M. A. Gates, Directional control of neurite outgrowth: emerging technologies for Parkinson's disease using magnetic nanoparticles and magnetic field gradients, J. R. Soc. Interface 19 (2022) 20220576, https://doi.org/10.1098/rsif.2022.0576.

[33] A. Falconieri, S. De Vincentiis, V. Cappello, D. Convertino, R. Das, S. Ghignoli, S. Figoli, S. Luin, F. Català-Castro, L. Marchetti, U. Borello, M. Krieg, V. Raffa, Axonal plasticity in response to active forces generated through magnetic nano-pulling, Cell Rep. 42 (2023) 111912, https://doi.org/10.1016/j.celrep.2022.111912.

[34] O. Yizhar, L.E. Fenno, T.J. Davidson, M. Mogri, K. Deisseroth, Optogenetics in Neural Systems, Neuron 71 (2011) 9–34.

[35] M. Sureda-Vives, K.S. Sarkisyan, Bioluminescence-driven optogenetics, Life 10 (2020) 1–11, https://doi.org/10.3390/life10120318.

[36] M.P. Calatayud, B. Sanz, V. Raffa, C. Riggio, M.R. Ibarra, G.F. Goya, The effect of surface charge of functionalized Fe3O4 nanoparticles on protein adsorption and cell uptake, Biomaterials 35 (2014) 6389–6399, https://doi.org/10.1016/j.biomaterials.2014.04.009.

[37] C. Riggio, M.P. Calatayud, M. Giannaccini, B. Sanz, T.E. Torres, R. Fernández-Pacheco, A. Ripoli, M.R. Ibarra, L. Dente, A. Cuschieri, G.F. Goya, V. Raffa, The orientation of the neuronal growth process can be directed via magnetic nanoparticles under an applied magnetic field, Nanomedicine Nanotechnology, Biol. Med. 10 (2014) 1549–1558, https://doi.org/10.1016/j.nano.2013.12.008.

[38] S. De Vincentiis, A. Falconieri, M. Mainardi, V. Cappello, V. Scribano, R. Bizzarri, B. Storti, L. Dente, M. Costa, V. Raffa, Extremely Low Forces Induce Extreme Axon Growth, J. Neurosci. 40 (2020) 4997–5007.

[39] Y. Wang, B. Li, H. Xu, S. Du, T. Liu, J. Ren, J. Zhang, H. Zhang, Y. Liu, L. Lu, Growth and elongation of axons through mechanical tension mediated by fuorescent-magnetic bifunctional Fe3O4·Rhodamine 6G@PDA superparticles, J. Nanobiotechnology 18 (2020) 1–18.

[40] Q. Goh, C.L. Dearth, J.T. Corbett, P. Pierre, D.N. Chadee, F.X. Pizza, Intercellular adhesion molecule-1 expression by skeletal muscle cells augments myogenesis, Exp. Cell Res. 331 (2015) 292–308, https://doi.org/10.1016/j.yexcr.2014.09.032.

[41] S. Li, J. Li, Y. Chun, P.K. Shrestha, X. Chang, M. Pivnenko, D. Chu, Variety of Ordered Patterns in Donor-Acceptor Polymer Semiconductor Films Crystallized from Solution, ACS Appl. Mater. Interfaces 13 (2021) 19055–19063, https://doi.org/10.1021/acsami.1c00079.

[42] S.R. Heidemann, D. Bray, Tension-driven axon assembly: a possible mechanism, Front. Cell. Neurosci. 9 (2015) 316, https://doi.org/10.3389/fncel.2015.00316.

[43] B.J. Pfister, A. Iwata, D.F. Meaney, D.H. Smith, Extreme stretch growth of integrated axons, J. Neurosci. 24 (2004) 7978–7983, https://doi.org/10.1523/JNEUROSCI.1974-04.2004.

[44] B.J. Pfister, D.P. Bonislawski, D.H. Smith, A.S. Cohen, Stretch-grown axons retain the ability to transmit active electrical signals, FEBS Lett 580 (2006) 3525–3531, https://doi.org/10.1016/j.febslet.2006.05.030.

[45] M.H. Magdesian, G.M. Lopez-Ayon, M. Mori, D. Boudreau, A. Goulet-Hanssens, R. Sanz, Y. Miyahara, C.J. Barrett, A.E. Fournier, Y. De Koninck, P. Grútter, Rapid mechanically controlled rewiring of neuronal circuits, J. Neurosci. 36 (2016) 979–987, https://doi.org/10.1523/JNEUROSCI.1667-15.2016.

[46] M.Jazvinšcak Jembrek, G. Šimic, P.R. Hof, S. Šegota, Atomic force microscopy as an advanced tool in neuroscience, Transl. Neurosci. 6 (2015) 117–130, https://doi.org/10.1515/tnsci-2015-0011.

[47] T.J. Gahl, A. Kunze, Force-mediating magnetic nanoparticles to engineer neuronal cell function, Front. Neurosci. (2018) 299, https://doi.org/10.3389/fnins.2018.00299.

[48] L. Miles, J. Powell, C. Kozak, Y. Song, Mechanosensitive Ion Channels, Axonal Growth, and Regeneration, Neuroscientist 29 (2023) 421–444, https://doi.org/10.1177/10738584221088575.

[49] M.A. Wheeler, C.J. Smith, M. Ottolini, B.S. Barker, A.M. Purohit, R.M. Grippo, R. P. Gaykema, A.J. Spano, M.P. Beenhakker, S. Kucenas, M.K. Patel, C.D. Deppmann, A.D. Güler, Genetically targeted magnetic control of the nervous system, Nat. Neurosci. 19 (2016) 756–761, https://doi.org/10.1038/nn.4265.

[50] J.K. Sethi, A. Vidal-Puig, Wnt signalling and the control of cellular metabolism, Biochem. J. 427 (2010) 1–17, https://doi.org/10.1042/BJ20091866.

[51] Y. Yang, M. Mlodzik, Wnt-Frizzled/Planar Cell Polarity Signaling: cellular Orientation by Facing the Wind (Wnt), Annu. Rev. Cell Dev. Biol. 31 (2015) 623–646, https://doi.org/10.1146/annurev-cellbio-100814-125315.

[52] X. Wang, Q. Liu, B. Zhang, Leveraging the complementary nature of RNA-Seq and shotgun proteomics data, Proteomics 14 (2014) 2676–2687, https://doi.org/10.1002/pmic.201400184.

[53] M.M. Shipley, C.A. Mangold, M.L. Szpara, Differentiation of the SH-SY5Y human neuroblastoma cell line, J. Vis. Exp. 108 (2016) 53193.

[54] F. Griese, P. Ludewig, F. Thieben, N. Gdaniec, T. Knopp, Imaging and moving magnetic beads with magnetic particle imaging for targeted drug delivery, in: Proc. - Int. Symp. Biomed. Imaging, 2018, pp. 1293–1296, https://doi.org/10.1109/ISBI.2018.8363808.